Institute of Biomechanics
Center of Biomedical Engineering
Kronesgasse 5-I
8010 Graz, Austria

Master's Thesis

Biomechanical Investigation of Human Abdominal Adipose Tissues: A Basis for Breast Reconstruction

to achieve the degree of
Master of Science

Author: Christoph Schwarz, BSc
Supervisor: Gerhard Sommer, PhD
Head of Institute: Professor Gerhard A. Holzapfel, PhD

November 5, 2013

Contents

Abstract

The demand for receiving treatment in plastic surgery is increasing for several reasons, e.g. breast reconstruction surgery with abdominal adipose tissue after carcinoma. Although these techniques are already performed in clinical practice, a detailed mechanical investigation can not be found in the literature. Hence, the aim of this project was to obtain multiaxial mechanical data of human abdominal adipose tissue. Moreover, the underlying microstructure of the tissue should be investigated. The biomechanical results were achieved by conducting both biaxial tension and triaxial shear tests at several stretch levels and amounts of shear, respectively. Additionally, relaxation and compression tests were performed. Although in past research projects not claimed, non-linear as well as anisotropic behavior was ubiquitous during all testing scenarios. The compression tests showed different stress levels in each direction. Furthermore, the investigation of the microstructure was achieved by a combination of optical clearing and Multi-Photon-Microscopy with Second Harmonic Generation sequencing. Data thus obtained showed a correlation with the results of both the biaxial tension and the triaxial shear tests. In the future, the results of this research might help discovering parameters of a constitutive model in the realm of nonlinear continuum mechanics. This material model together with the parameter could be included into a finite element model, to perform simulations. Such computer simulations will help doctors find the best surgical procedure for the optimal breast restoration and surgical outcome.

Die Nachfrage nach plastischen Eingriffen in der Medizin steigt von Jahr zu Jahr an. Bei den zur Rekonstruktion bestimmter Körperregionen (Brust nach Brustkrebs) verwendeten Materialien, handelt es sich oft um menschliches Bauchfettgewebe. Das Ziel dieses Projektes war es statistisch gute multiaxiale mechanische Daten dieses Gewebes zu erhalten. Zusätzlich wurden Strukturuntersuchungen, unter Verwendung einer derzeit aktuellen bildgebenden Technik, durchgeführt. Die mechanischen Daten wurden durch Testen des Gewebes sowohl mittels biaxialen Zugversuchen als auch triaxialen Scherversuchen erhalten. Des Weiteren wurden ein Relaxationstest und ein Kompressionsversuch nach den zyklischen Scherversuchen einer Probe durchgeführt. Die Ergebnisse aller Tests zeigten ein nichtlineares und anisotropes Verhalten. Speziell der Kompressionsversuch zeigte deutliche Unterschiede der maximalen Spannungswerte in die unterschiedlichen Richtungen. Die Ergebnisse der Multi-Photonen-Mikroskopie Untersuchung befestigten die erhaltenen Resultate der biaxialen Zug- und triaxialen Scherversuche. Diese gewonnenen Daten können nun zur Bestimmung von Materialparametern verwendet werden. Mit diesen Materialparametern und dem zugehörigen Materialmodell können Finite Elemente Meth-

ode (FEM)-Simulationen durchgeführt werden. In naher Zukunft könnten diese FEM-Simulationen zur Entwicklung eines Computerprogramms verwendet werden, um eine Hilfestellung und Unterstützung von Ärzten und Chirurgen in relevanten Gesundheitsfragen darzustellen.

Acknowledgment

The main gratefulness I am in debt to my parents, who always supported my decisions, both good and bad ones. I would never have had the opportunity to attend such an education without their full mental and financial support. I am thankful for their guidance on my way to become who I am now. Further I want to thank my Supervisor Gerhard Sommer, PhD, who always supported me at my work and all other problems that came up during this time. Moreover I want to thank the head of the Institute of Biomechanics, at Graz University of Technology, Prof. Gerhard Holzapfel, PhD, for providing the laboratory facilities as well as all other institutional supplied materials.
A great benefit was the support of Heimo Wolinski, PhD, of the Institute of Molecular Bioscience at the University of Graz, who supported me duringthe Multi-Photon-Microscopy imaging with his knowledge.
I am also thankful to Maximilian Eder, PhD, and Christoph Müller, MSc who were responsible for the sourcing the samples and funding this research project, respectively.
Further I want to thank my uncle Prof. Heinz Sill, PhD, who helped and supported me establishing contacts to the Institute of Pathology of Medical University Graz, which was a big jigsaw piece in achieving the expected number of samples.
I also want to express my gratitude to Prof. Peter Regitnig, PhD, and Prof. Gerald Höfler, PhD, from the Institute of Pathology of Medical University Graz, for acquiring a number of samples as well as helping me during the preparation for the ethics proposal.

1. Introduction

1.1. Motivation

In the last 20 years society has aimed to increase its knowledge about the human body as well as about each single fragment itself. In summary, one should know that some of the tissues within the human body were investigated more than others. Mechanically, human adipose tissue has largely been not examined compared to others, e.g. arterial tissue. Nevertheless, the significance of the knowledge of human abdominal adipose tissue has increased within the last decade, particularly because of the medical field of aesthetic surgery. Indeed, plastic surgeons started to use patient's own adipose tissue for several reconstructive operations, e.g. for breast reconstruction after the removal of the breast because of malign breast cancer. For scientists the mechanical properties of human adipose tissue are desirable, primarily for the reason of getting a better understanding of whether adipose tissue is an appropriate material for substituting the former tissue. Although the application is already executed in hospitals, a detailed biomechanical characterization of the tissue is largely unidentified. Nevertheless, for a detailed pre-surgical clarification as well as a basis for a good computer simulation, which should support doctor's decisions, it is essential to gain more information about this part of the human body. Therefore, the first step in the chain of increasing the understanding of the whole tissue is to obtain the detailed mechanical properties. Subsequently after a number of samples, which should not be too low to reduce the variance and gain statistically good results, were tested in the lab. Afterward, the experimentally gained data can be fitted to constitutive equations through the realm of nonlinear continuum mechanics (e.g. Holzapfel et al. (2000)). The next steps could be an implementation into a finite element application which could then lead into a computer simulation that might be used in clinical practice. This computer simulations might be able to give a good prediction of the surgical success as well as to generate a better illustration to the patient and the doctor.

1.2. Human Abdominal Adipose Tissue

The next paragraphs describe the basics of human adipose tissue. In addition to this structural information one can find an explanation of the assumed geometrical characteristics and the underlying nomenclature, which was used in this project.

1.2.1. Basics and Main Functionality

As with all types of biological tissue, human adipose tissue has its own particular characteristics. Every human being has adipose tissue on several locations within the body.

Some adipose deposits are absolutely inevitable for a healthy person, e.g. fat pads in the feet or beyond the eye socket. Other types of fat signify unhealthy living, if the amount of adipose tissue gets too high, e.g. large stomach or a lot of adipose tissue at the upper arms. In general, the area underneath the skin of a human body consists of many different parts e.g. nerves, hair follicles, blood vessels and some more (see Fig. 1.1 for more detailed composition). Amongst others adipose tissue is one part that can be found in the dermis and in the hypodermis. Normally, it is a loose tissue that contains mostly of adipocytes (fat cells). There are two types of adipose tissue, brown adipose tissue and white adipose tissue, which comprise two types of fat cells. Mostly, if people talk about adipose tissue they think of white adipose tissue. This type can be found in almost every region of the human body embedded in the loose connective tissue.

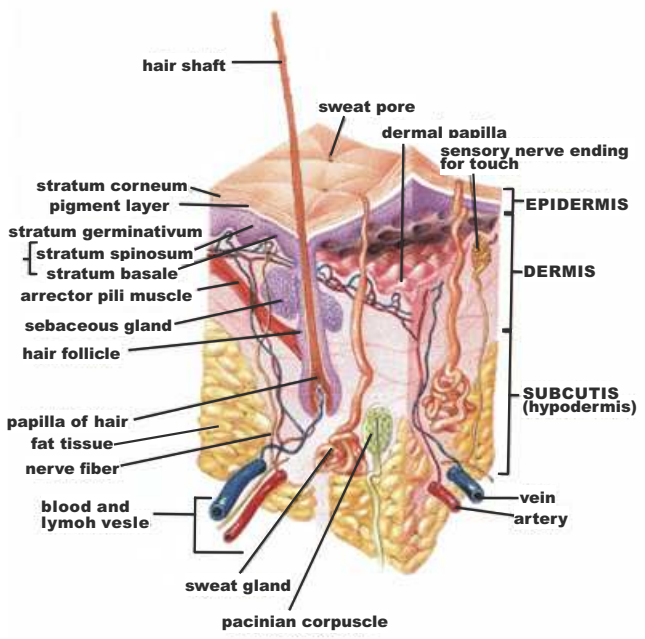

Figure 1.1.: Detailed description of the composition of the underlying layers beyond the skin. In this part of the body we can find nerves and nerve endings, muscles, arteries and veins hair follicles as well as adipose tissue and many others SEER (2013).

The white adipose tissue has to fulfill three main functions:

i) Fat storage: A human can survive up to 40 days (peak value) without eating anything. This can be achieved because every human being, varying on age and gender, has a certain amount of fat. This is usually around 10% (for sports-persons and athletes), up to $15 - 25\%$ (for a normal person) and high level obesity can be as high as 50%.

ii) Insulator: Adipose tissue has very poor heat conducting characteristics. Therefore, this type of material is perfect to help maintaining the body's temperature at $37°\mathrm{C}$.

iii) Constructive fat: In some parts of the body adipose tissue is used as a protection for other organ or underlying parts that are not capable of bearing high force and stresses, e.g. at the root base, buttocks or cartilages.

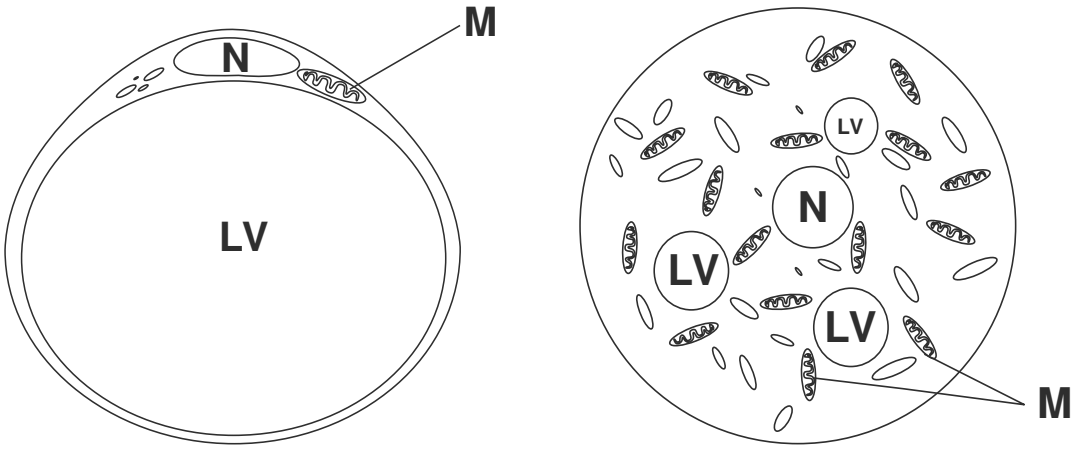

Figure 1.2.: Comparison between the two types of adipocytes, the white (a) and the brown (b) in a schematic image that shows the most important parts of the fat cells. LV: lipid vacuole, N: nucleus, M: mitochondria, the other parts stand for the leftovers within the cell. Pictures adopted from http://www.sportsci.org/encyc/adipose/adipose.html.

However, brown fat tissue is largely unnoticed in adults, and appears mostly in infants or animals. Brown adipose tissue can directly produce heat from the stored adipose tissue. In general, fat cells are reproduced all the time in the human body. An adipocyte of the white fat tissue is a single, large droplet with a maximum size up to $100\ \mu\mathrm{m}$ (Abrahamson 1986). The nucleus is situated on the edge of the cell because of the cell's large vacuole. Each adipocyte is enclosed by a basal lamina which is about $2\ \mu\mathrm{m}$ thick (Nakajima et al. 1998), and contains the proteins collagen type IV, laminin and reticular collagen fibrils. In addition to the adipocytes there are thick bundles of collagen fibers called interlobular septa. We assume that these fibers, which are made of collagen type I and IV, are preferentially orientated into the longitudinal direction. This would make sense in order to absorb the earth's gravitational force, which is acting on the human body all the time and because of mechanobiological remodeling the tissue changes due to environmental influences. Contrary, the fat cells of the brown adipose tissue are smaller compared to the white adipocytes. The brown color of the tissue results from the higher number of mitochondria and the numerous amounts of smaller droplets.

1.2.2. Past Investigation and Obtained Mechanical Knowledge

The next few paragraphs present some of the past research projects concerned with adipose tissue of human as well as animals. One mechanical investigation of human calcaneal

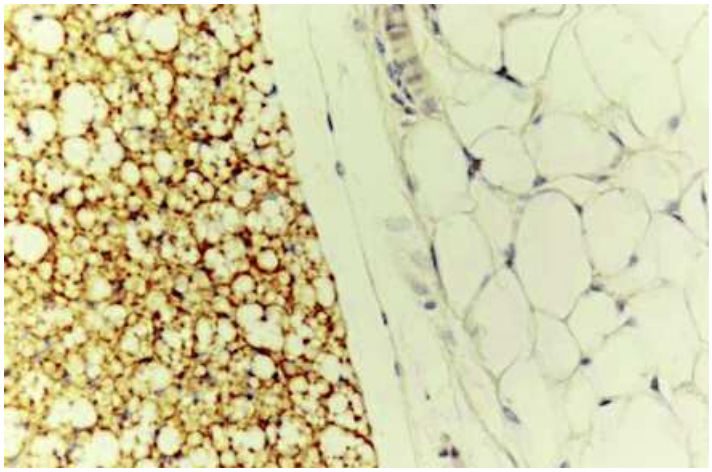

Figure 1.3.: Difference between the two types of fat; on the left side the brown and on the right side the white fat tissue. Image taken from Tam et al. (2012).

fat tissue was conducted by Miller-Young et al. (2002). They performed three types of compression tests on five cylindrical-shaped specimens of each patient: (i) a quasi-static (QS) compression test to determine the hyper-elastic properties; (ii) a stress-relaxation test to obtain the visco-elastic properties; and (iii) a rapid compression test at 175 and 300 mm/s. The results of all tests showed a non-linear behavior of the heel pad tissue.
Wu et al. (2007) investigated the behavior of a cylindrical shaped specimen of the adipose tissue and the skin under compression load. To distinguish the border between fat and skin tissue they used stains. They found that the stress-strain relationship depends on the height ratio of skin/subcutaneous tissue. Despite some scattering there is a trend in evidence. The three typical stages of soft biological tissue were defined as toe region, transient region and high stiffness region. The transient state from low to high stiffness occurs at strains of 0.3 and 0.4 for skin and subcutaneous tissue, respectively.
Samani et al. (2007) used an indentation technique to obtain the elastic modulus of human breast tissue. They developed two systems to measure Young's modulus of small samples for normal breast and one for tumorous tissue, respectively. One of their results was that most cancers had a higher Young's modulus than normal (healthy) fibroglandular fat tissue only.
In the work of Geerligs et al. (2008), porcine back adipose tissue was divided into an outer, middle and inner layer. After the preparation the specimen was tested in a rotational rheometer with strain control mode. Additionally, they applied the results to a material model. Moreover, they preformed histological examination to investigate the damages caused by freezing fat tissue. Among other things they found out that there exists an obvious temperature dependency and that the freezing of the tissue has no effect on its structure.
Comley and Fleck (2010) investigated porcine adipose tissue by executing a trouser tear test (so called because of the specimen looks like a trouser), where the two legs were pulled apart with a constant displacement rate $\dot{u}$ between 0.01 and 10 mm/s. The tests show that

for each value of $\dot{u}$ the force F increases with u and they oscillate about a value $\overline{F}$. Further they calculate some toughness values J_C.
Comley and Fleck (2010) had conducted another research project, where they investigated the uniaxial compression response. The goal of their work was to predict stresses over a range of strains that occur in the tissue during standardized medical application, e.g. needle injection. They chose porcine adipose tissue instead of human adipose tissue for several reasons, e.g. ethical or practical. They performed three types of compression tests, similar to Miller-Young et al. (2002) : (i) at low below 2 s^{-1}, (ii) at intermediate ($20 - 260$ s^{-1}) and (iii) at high strain rate (above 1000 s^{-1}). They remarked that the shape of the curves was similar through all strain rates, differing only in a form factor. Another conclusion was that the tissue behaves as a linear visco-elastic solid at small strain magnitudes over all frequencies up to 100 Hz.
Orbital fat tissue of porcine as well as of human was investigated by Chen and Weiland (2011) in a tensile test (v$=1.5$mm/s) at *in-vivo* conditions in $37°$C$\pm 1°$C saline. After obtaining the experimental data, they fitted the single linear, neo-Hookean and Mooney-Rivlin models as well as possible. Their main result was that there was no significant difference among the properties in the different directions in either the human or the porcine sample.
Conclusively the previous investigations have not dealt with human abdominal adipose tissue. The investigation of this tissue is absolutely desirable because it is already used in surgery. In addition there are no research groups who have investigated the biological material in all three directions. Lastly, the combination of the experimental data of the laboratory has never been combined with structural investigations. Our work combines the mechanical (both biaxial and triaxial) investigation of human abdominal adipose tissue with structural investigation.

2. Materials and Methods

The following section describes the main facts concerning the utilized adipose tissue, i.e. the preparation work, the used experimental setups and the conducted testing protocols. Additionally, in this section an introduction into the mechanical theory of biaxial tension and triaxial shear testing is given. Further, the preparation for the microstructural investigation and the theory of Multi-Photon-Microscopy (MPM) are described.

2.1. Material - Human Abdominal Adipose Tissue

The human adipose tissue is removed from female patients during plastic surgery. There are several reasons for such a surgery, e.g. breast reconstruction after a mamma carcinoma or abdominoplasty because of the patient's personal preference. The remaining part of the tissue is directly sent to our laboratory so that it can be tested as fresh as possible. Figure 2.1 shows the approximate region where the adipose tissue is removed. During the transport the fat tissue is packed into a small container, which is filled with a Phosphate-Buffered-Saline (PBS) solution. This container is packed into a larger box which is filled with dry ice to cool the tissue during shipping. All personal information of the patients were treated as confidential, important and interesting facts were made anonymous and are shown in Table 2.1. This reveals, for instance, the age, height, weight and more facts which may be of interest.
After receiving the sample in the laboratory, the first step after unwrapping the whole package is to decide whether it is possible to conduct both biaxial tension and triaxial shear test or just one of them, in regards to the size of the biological tissue sample (see Fig. 2.2). It must be mentioned that the whole preparation is performed incipient at the innermost side of the tissue (not at the epidermis' side). The first slice of about 3 mm of the tissue must be removed with an electrical cutting-device, which has to be humidified with PBS solution so that the tissue does not stick to the blade of the slicer. The first slice of the tissue cannot be used for the experiment due to the inconstant thickness. Hence, this piece is just cut off to straighten the surface to ensure constant thickness of the specimens.

2.1.1. Geometry in the Human Body

At the beginning of the experimental analysis of the tissue, definition of the orientation in the human body has to be established and may not be changed again due to avoid confusions. This is a very important step. It should be written down and be preserved during the whole investigation. Further, the orientation is necessary for the interpretation of the results of the mechanical as well as of the structural part. Our considerations led to the

Table 2.1.: Information to the received and tested adipose tissue (e.g. age and weight). f..female, b..biaxial tensile, t..triaxial shear, r..right, l..left, m..middle, m-l..mid left
* specimens received from the Institute of Pathology at Medical University Graz.

Sample No.	Sex	Age y	Height cm	Weight kg	BMI kg/m^2	Testtype(s)	Removal region	
I	f	22	175	82	27	b + t	r	
II	f	64	169	96	34	b + t	r	
III	f	75	178	72	23	t	r	
IV	f	50	175	73	24	b + t	r	
V	f	49	168	70	25	b + t	r	
VI	f	28	166	68	25	b + t	l	
VII	f	57	164	72	27	b + t	r and m	
$VIII$	f	44	165	70	26	b + t	r	
IX	f	30	164	60	22	b	m-l	
X	f	30	164	60	22	b + t	r and l	
XI	f	27	159	55	22	b	l	
XII	f	30	165	85	31	b	l	
$XIII$	f	30	165	200	73	b	l	
XIV	f	72	175	75	24	b	l	*
XV	f	79	165	73	27	b + t	l	*
XVI	f	72	162	72	27	b + t	m-l	*
mean		48.5	166.94	79.41	28.59			
SD		4.67	1.33	7.65	2.79			

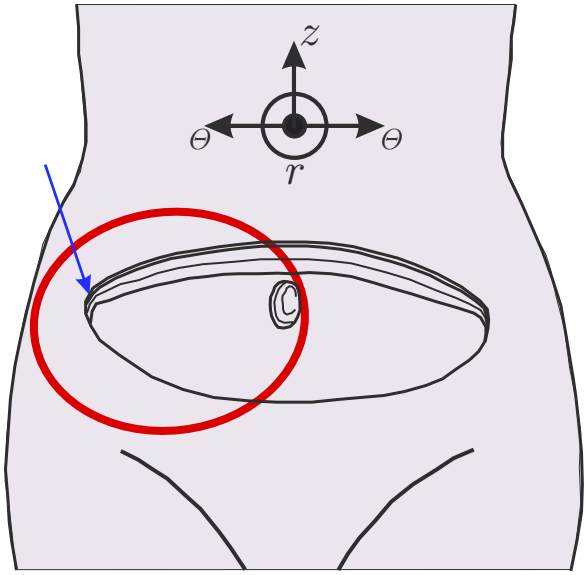

Figure 2.1.: Schematic illustration of the region where the adipose tissue was removed of the patient's abdomen. Red..signifies the removed side; blue..the arrow stands for the suture material marker in the tissue that indicates the outer side of the sample.

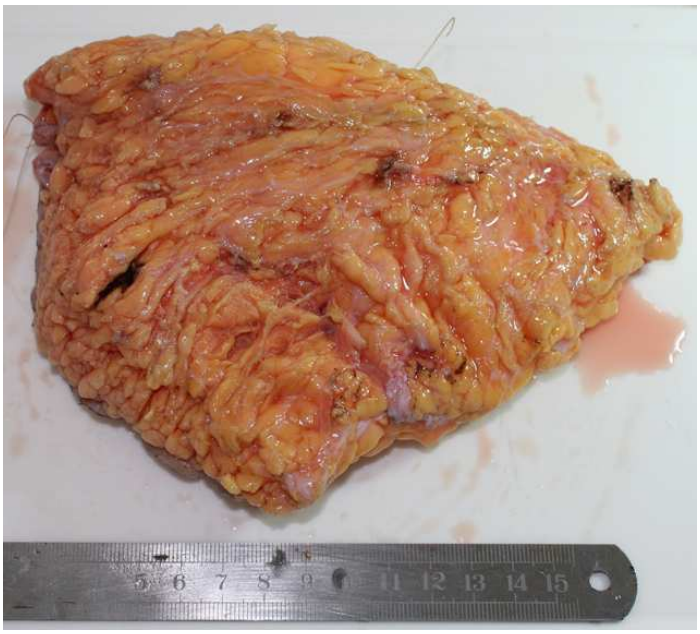

Figure 2.2.: Representative adipose tissue sample, viewed form the backside, after the reception in the laboratory.

assumption that the human body has, from the centric vertically body-axis' point of view, more or less a symmetrical shape. Therefore, the transversal direction (θ-direction) goes both into the right and the left from the centric axis of the person towards the outside. The positive longitudinal direction (z-direction) is defined cranial towards the head. The definition of the third direction of the adipose tissue within the trunk is the sagittal direction (r-direction). It goes from the inside of the human body, where the organs lie, towards the outside where the epidermis is located. Because of this special orientation definition, it is absolutely unavoidable to get a detailed description of the surgeon, where the sample was extracted. To simplify the written explanation of the chosen orientation the reader is referred to Fig. 2.3.

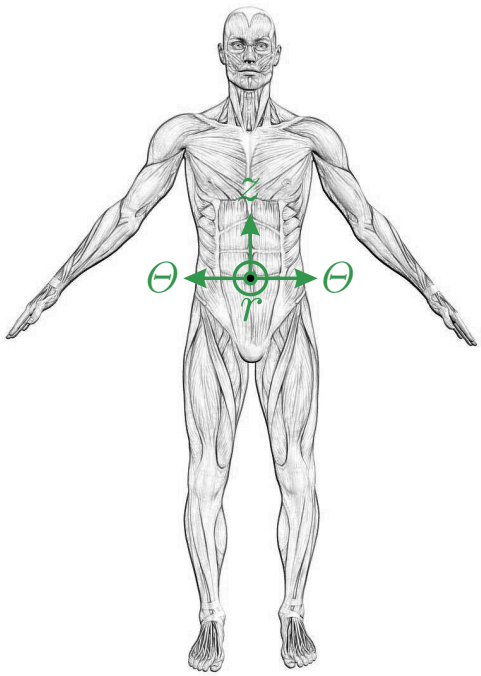

Figure 2.3.: Definition of the used orientation of the sample of adipose tissue within the human body (image adopted from http://what-when-how.com/wp-content/uploads/2012/08/).

2.2. Biaxial Tensile Test

2.2.1. Preparations

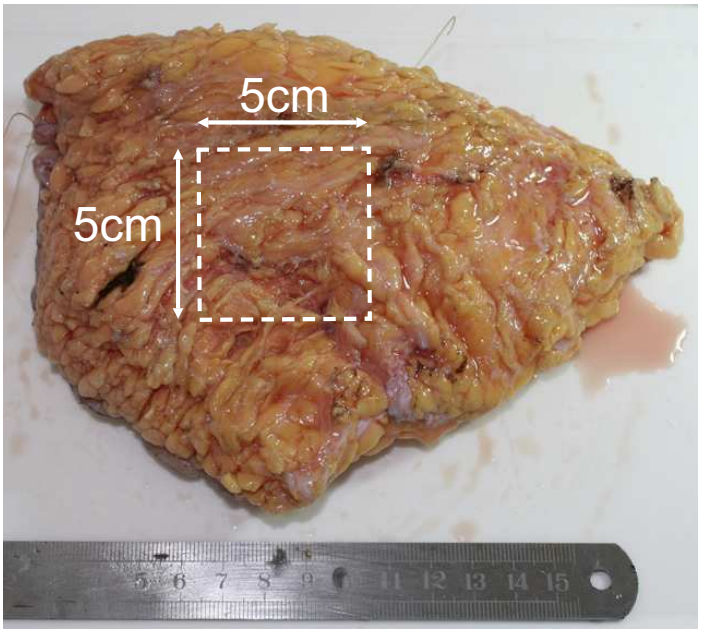

Figure 2.4.: A 5 mm thin slice is cut out of the tissue in order to cut a 5×5 cm piece out of this slice.

The biaxial tensile test requires a squared specimen of about 5×5 cm (see Fig. 2.4) and a thickness of approximately 5 mm (to gain a ratio of about $10{:}1$ between the side lengths and the thickness). A specimen for biaxial testing was prepared of the whole fat sample by the usage of an electrical slicer, a 5×5 cm metal stencil, a sharp blade and a scalpel. Thereafter, a 5×5 cm quadratic piece can be prepared. In order to achieve a straight and clean cut at the demanded geometry, all tasks were executed step-by-step, where the sample was cooled (~$2°$C) before each step.

The next step was the fixation of the four clamps at the edges of the squared tissue specimen (see the schematic in Fig. 2.5a). Therefore, a commercially obtainable cyanoacrylate gel adhesive was used. After this procedure, the distance between the clamps in both directions must be measured exactly with a scale for stress calculations. As you can see in Fig. 2.5b the clamps with its connected yarns were used to insert the specimen into the testing device. In the end, nine markers were applied within an 1×1 cm area in the center of the tissue sample also by using the same super-glue. The used markers were made out of a black foam rubber material which is known to have good non-reflective characteristics, which is a very useful property in our field of application. The finished prepared specimen was put in a glass container filled with PBS solution at $37°$C by a heating circulation unit. Afterwards the specimen was fixed to the actuators by yarns and clamps. A glass mounted

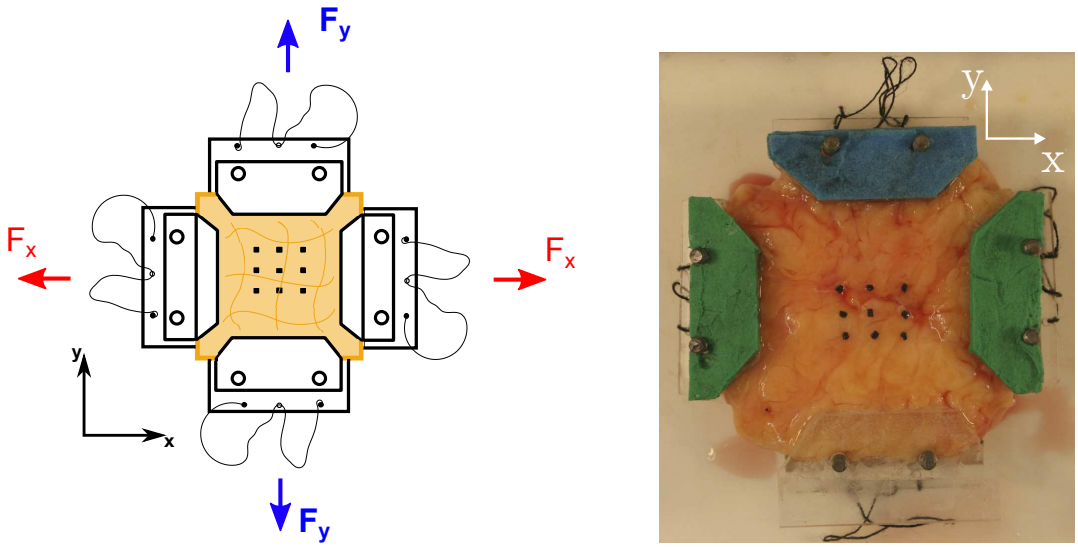

(a) (b)

Figure 2.5.: (a) Schematic description of the correctly for the biaxial test prepared adipose tissue (including the deformation markers as well as the clamps for fixation). (b) Biaxial tissue specimen after finishing the preparation work. Nine markers are spotted in the middle of the specimen. Outside the clamps there are special mounted yarns to insert the specimen in the biaxial tension testing apparatus.

on a swiveling arm (see Fig. 2.6) was positioned directly at the solution's surface, including a small angle between the PBS and the surface of the glass (there is contact between the solution and the glass) to avoid reflection on the liquid's surface caused by the lights, which is necessary for the video-extensometer to detect the markers correctly.

2.2.2. Testing Protocols

After finishing all parts of the preliminary arrangements, the next step was the actual testing. The biaxial experiments were separated into several divisions. In principle, different stretches (λ from 1.05 to 1.20 in 0.05 steps unless the specimen ruptures) were applied onto the specimen consecutively, in both the x- and the y-direction of the apparatus simultaneously (this we call a stretch-controlled protocol). These stretches induce stresses within the tissue in both directions. The resulting forces were measured by four loading cells (two in each direction) situated in the actuator arms of the apparatus. A camera located about 30 cm above the testing area is used to monitor the deformation of the tissue by capturing the markers with a video extensometer software (Laser Speckle Extensometer Version 2.23.3.0 by Messphysik Material Testing). This software was also linked with the test control software (Test & Motion Version 2.0 by DOLI Electronic GMBH). The adipose tissue was preconditioned with four consecutive cycles at the beginning of each stretch value. Afterwards, the test at quasi-static conditions at different ratios of the stretch in the two directions (1:1, 1:0.75, 0.75:1, 1:0.5 and 0.5:1) was conducted, whereat each

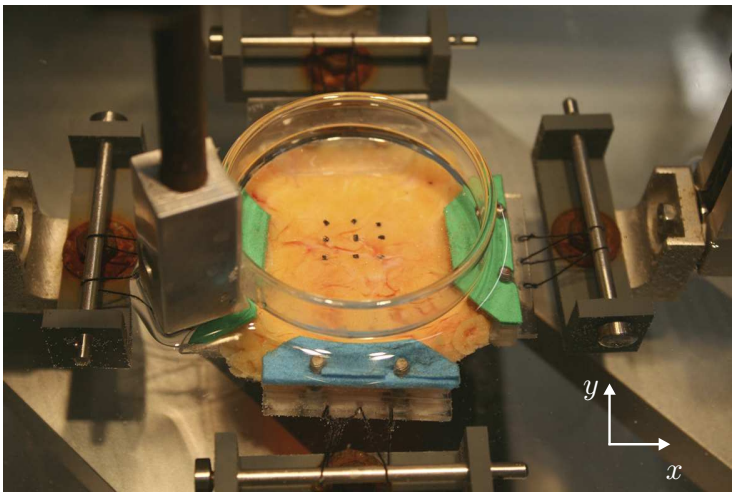

Figure 2.6.: Tissue sample already inserted into the biaxial testing apparatus. Also shown is the partly submerged glas to minimize reflections on the fluid's surface by the used lights.

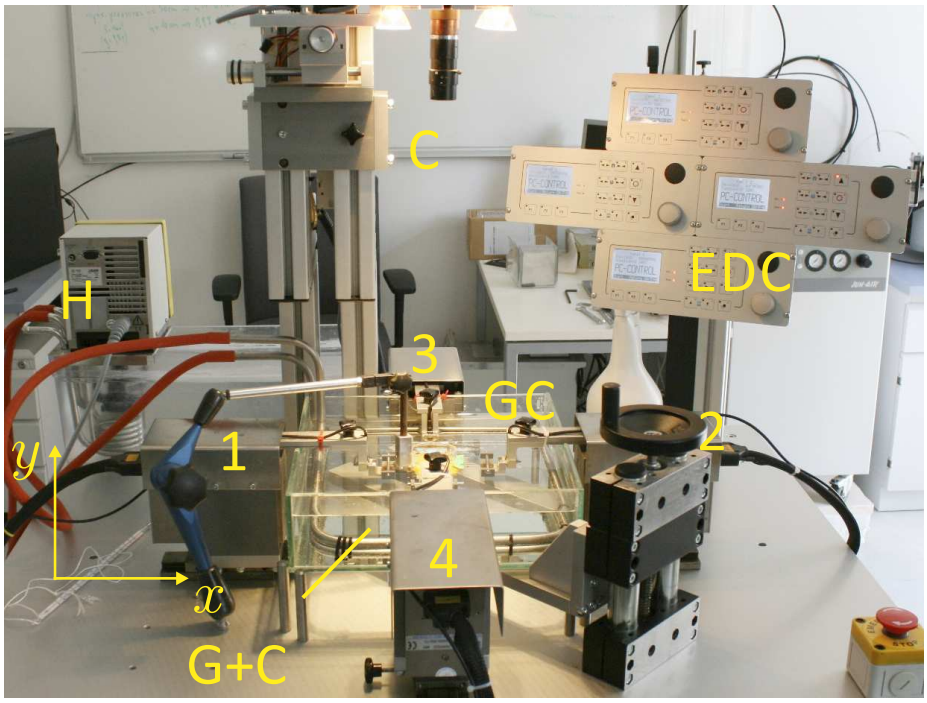

Figure 2.7.: Overview of the biaxial tension testing apparatus (Graz University of Technology and Messphyisk). The numbers 1 to 4 at the linear actuators denominate the loading cells which are responsible for measuring the acting force for the applied stretches. C..camera, G+S..glass and specimen, EDC..electronic digital controllers, GC..glass container and H..heating circulation unit

ratio includes one loading-unloading cycle. The speed of these loading- and unloading-cycles was chosen to be QS, v=8mm/min for the measurement as well as for preconditioning. After completion of the tests at different stretch-rates and ratios, a dynamic test at higher speed (v=50mm/min) and at a ratio of 1:1 was conducted. An earlier abortion of the whole experiment was not in plan and could only be caused if the specimen got torn out of one of the clamps or got ruptured, so that a further testing was not possible. After testing, the thickness of the specimen was determined by a video-extensometer (used software is Videoextensometer NG Version 5.26.0.0 SP3 by Messphysik Material Testing). This last step has to be conducted to calculate the stresses of the recorded force data for the interpretation of data.

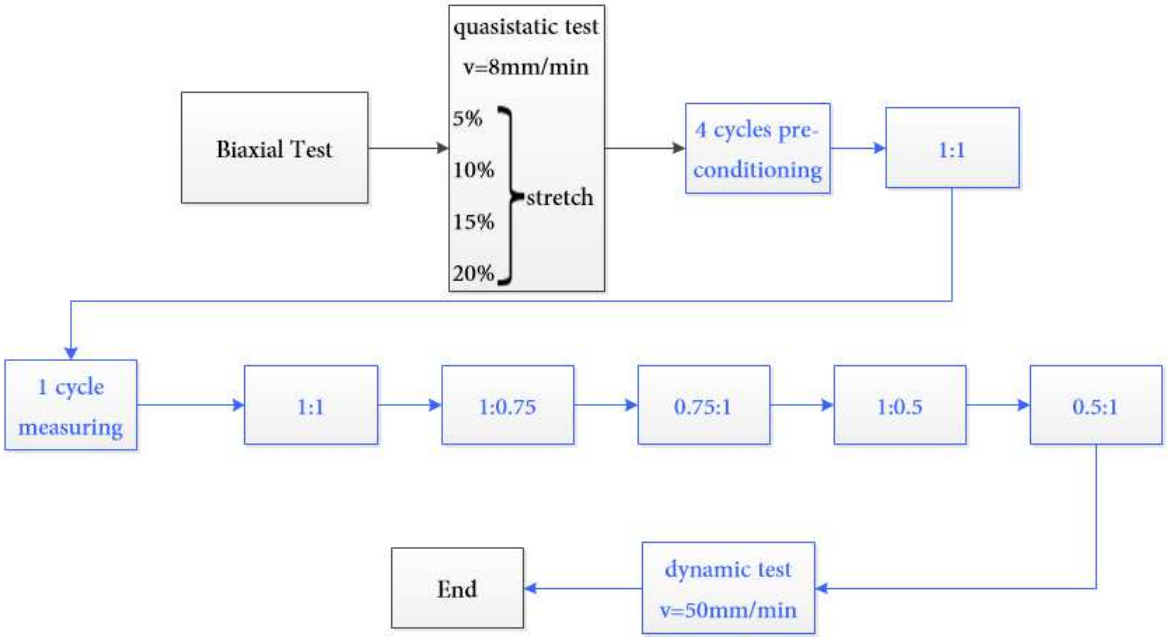

Figure 2.8.: Flow-chart showing the workflow of the biaxial tensile test. The blue part of the diagram is performed at each stretch value.

2.2.3. Theoretical Background

The theory of the biaxial tension tests can described in the realm of nonlinear continuum mechanics. Well known on this field is the deformation gradient, which is defined as

$$\mathbf{F}(\mathbf{X},t) = \frac{\partial \chi(\mathbf{X},t)}{\partial \mathbf{X}} = \mathbf{x}(\mathbf{X},\mathrm{t}). \tag{2.1}$$

Another notation which is written in Humphrey et al. (1990) appears in this form

$$\mathbf{F} = \mathbf{I} + \mathrm{Grad}(\mathbf{U}) \tag{2.2}$$

where $\mathrm{Grad}(\mathbf{U})$ is the formulation for the displacement field and $\mathbf{I}$ is the unity tensor. Written in form of components follows

$$\begin{aligned} F_{11} &= \lambda_1 = 1 + \frac{\partial u_1}{\partial X_1} \\ F_{12} &= \kappa_1 = \frac{\partial u_1}{\partial X_2} \\ F_{21} &= \kappa_2 = \frac{\partial u_2}{\partial X_1} \\ F_{22} &= \lambda_2 = 1 + \frac{\partial u_2}{\partial X_2} \end{aligned} \tag{2.3}$$

where λ_i $(i = 1, 2)$ are stretch ratios and κ_j $(j = 1, 2)$ are measures of shear. The last component F_{33} can be calculated by assuming incompressibility ($J = \det \mathbf{F} = 1$), results in

$$F_{33} = \lambda_3 = 1/(\lambda_1\lambda_2 - \kappa_1\kappa_2). \tag{2.4}$$

In matrix form the deformation gradient is

$$\mathbf{F} = \begin{bmatrix} \lambda_1 & \kappa_1 & \sim 0 \\ \kappa_2 & \lambda_2 & \sim 0 \\ \sim 0 & \sim 0 & \lambda_3 \end{bmatrix}. \tag{2.5}$$

Hence, the formulation for the first Piola-Kirchhoff stress tensor $\mathbf{P}$ can be used to obtain the Cauchy stress tensor $\boldsymbol{\sigma}$ as

$$\boldsymbol{\sigma} = (1/\det \mathbf{F})\mathbf{F}\mathbf{P} = \left(\frac{1}{J}\right)\mathbf{F}\mathbf{P}. \tag{2.6}$$

Since it is assumed that the testing is conducted in plain conditions (means that $t_{i3} = 0$) the first Piola-Kirchoff tensor in component notation is

$$\begin{aligned}\sigma_{11} &= \lambda_1 P_{11} + \kappa_1 P_{21}\\ \sigma_{22} &= \lambda_2 P_{22} + \kappa_2 P_{12}\\ \sigma_{12} &= \lambda_1 P_{12} + \kappa_1 P_{22}\\ \sigma_{21} &= \lambda_2 P_{21} + \kappa_2 P_{11}\end{aligned} \tag{2.7}$$

whereat $\sigma_{12} = \sigma_{21}$ because of the second Cauchy's law of motion. Assuming P_{12} and P_{21} are approximately zero (see Humphrey et al. (1990)) and σ_{11} and σ_{22} are determinable values of the forces of the biaxial tension setup, the normal components of $\boldsymbol{\sigma}$ can easily be calculated

$$\begin{aligned}\sigma_{11} &= \lambda_1 P_{11} = \lambda_1 (f_1 / A_2)\\ \sigma_{22} &= \lambda_2 P_{22} = \lambda_2 (f_2 / A_1)\end{aligned} \tag{2.8}$$

with A_k $(k = 1, 2)$ is the initial area (composed of the orthogonal side and the thickness of the specimen), whereas the forces f_n $(n = 1, 2)$ in the respective direction affect. Although the two first Piola-Kirchhoff stresses P_{12} and P_{21} are assumed to be zero, the shear parts of the Cauchy stress are non-zero because κ_j $(j = 1, 2)$ are also non-zero. The affected areas are calculated from the measured reference thickness and the distance between the clamps in both directions.

2.3. Triaxial Shear Test

2.3.1. Preparations

To obtain the data of a complete triaxial shear test, it is essential to execute all six possible shear modes. Two shear modes (Fig 2.9) can be executed consecutively with one $8{\times}8{\times}8$ mm cube of tissue. In summary, three of those cubes have to be dissected out of the whole adipose tissue. To achieve this size as accurately as possible, there are a few preparation steps that have to be executed. First, it is necessary to cut an 8 mm thick slice of the tissue by using the electrical cutting device (here the 3 mm slice for smoothing the tissue's surface has to be cut already). The following step is to cut a long piece with a width of 8 mm out of the slice (Fig. 2.10). Subsequently, the three (or more if more than one complete triaxial shear test is executed) $8{\times}8{\times}8$ mm cubes can be easily cut from the rectangular-shaped fat tissue. Similarly as the preparation of the biaxial specimen, it is necessary to cool the tissue sample in the freezer (~2°C) to ensure an exact and straight cut using the slicer, the scalpel, or the sharp blade.

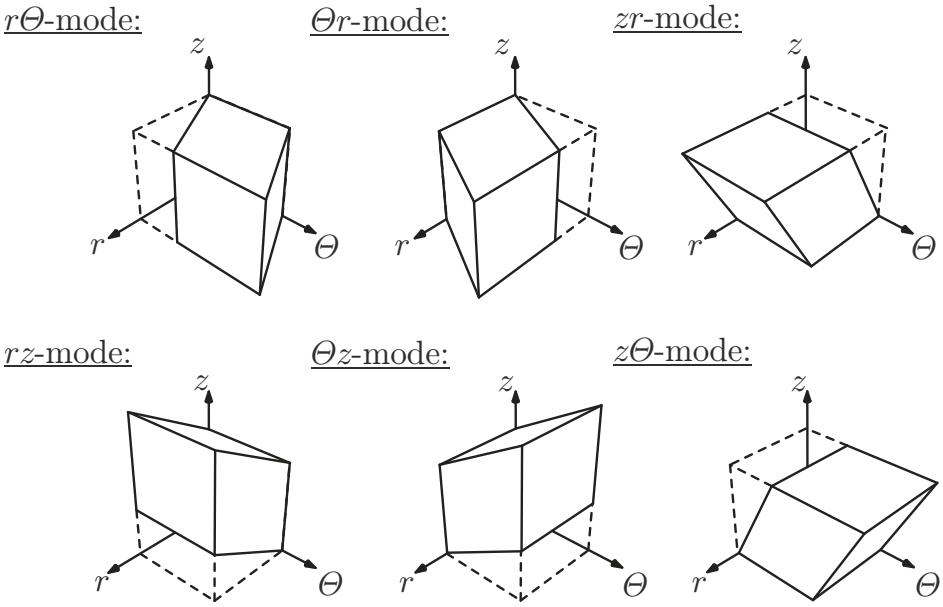

Figure 2.9.: Six different shear modes for the description of the shear behavior of the adipose tissue. Labeling of the axes is shown in the human configuration (r, θ, z).

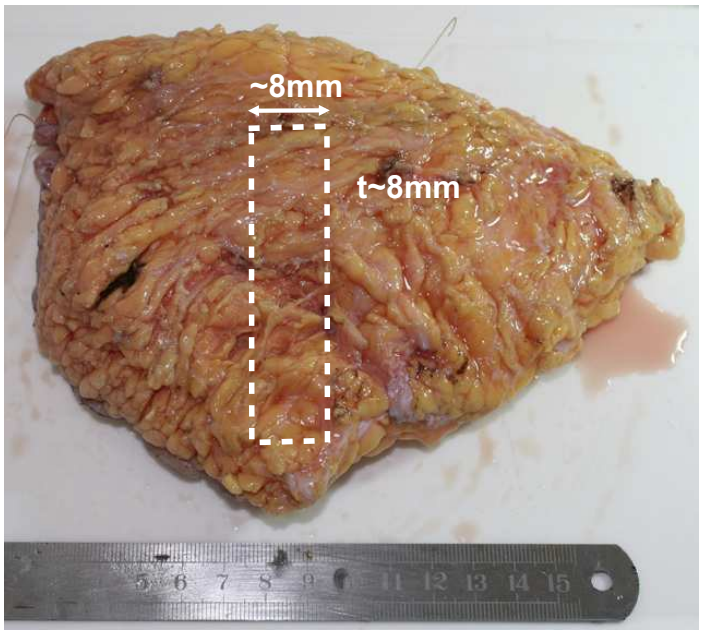

Figure 2.10.: Adipose sample obtained form - showing the location and the size of the long rectangular piece for the specimen preparation.

The cube-shaped specimen must now be fixated on the mounting device of the triaxial testing setup (Fig. 2.11). As adhesive a commercially available super-glue was used, like it was for the biaxial tests. Using this cylindrical mounting device made of metal it was very easy to place the specimen into the triaxial testing device (Graz University of Technology and Zwick & Roell) by flipping it $180°$ over the y-axis of the machine (for description of the axis system of the apparatus see Fig. 2.12 and the section below). The preparation of one specimen is accomplished when it is attached on both top and bottom in the testing device's mountings. After this, small glass container which surrounds the apparatus and the specimen during the experiment has to be filled with a PBS solution of $37°$C so that the whole specimen is covered (Fig. 2.12). Similar to the biaxial tensile test, the solution is heated to keep its temperature. After finishing all previously mentioned steps the actual testing sequence can be started.

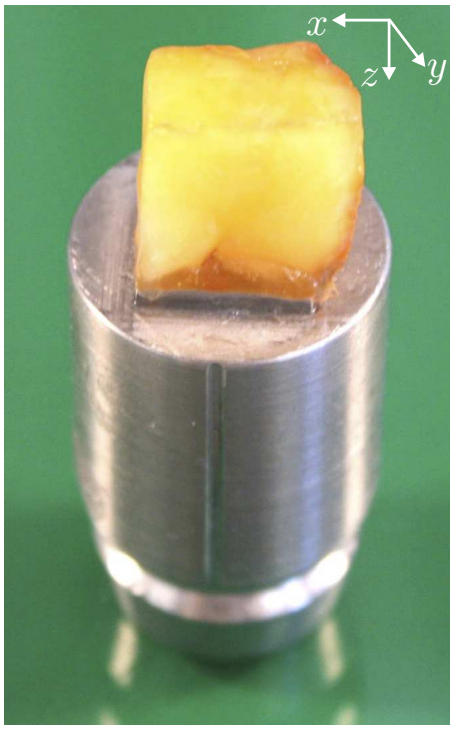

Figure 2.11.: The specimen is fixed with super-glue on the cylindrical mounting device of the triaxial apparatus. The attachment is standing upside down and must be rotated 180° in y-direction to plug it into the testing apparatus.

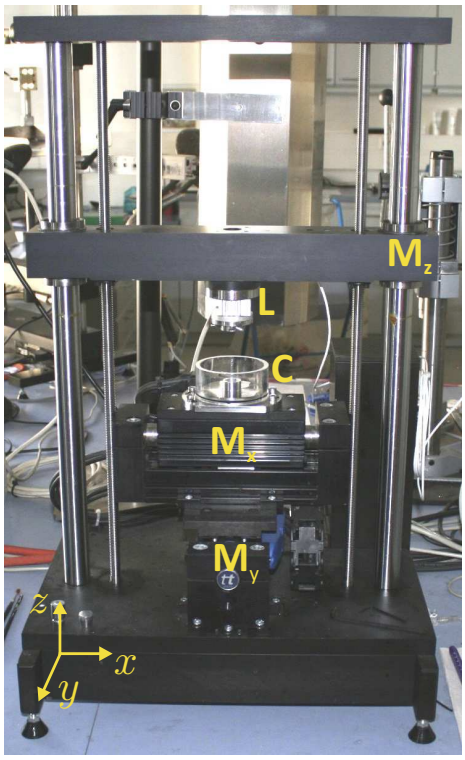

Figure 2.12.: The triaxial testing apparatus. M_x, M_y, M_z..linear actuator in x-, y- and z-direction, respectively, L..3-axes-load cell (force transducer), C..container for PBS solution and deposition for the specimen in the center.

2.3.2. Testing Protocol

At the beginning of the experiment, the exact geometrical dimensions of the cube-shaped specimen must be entered into the software (TestXpert II Version 3.2 by Zwick & Roell), which controls the device. In this part the axis labeling was written in form of the testing apparatus (x, y, z coordinates; whereas r, θ, z is the notation for the tissue orientation). The complete sequence was split into four different parts, where each of them was conducted at a different amount of shear (20%, 30%, 40% and 50%). At each step the specimen was preconditioned previously. Thereby two loading- and unloading-cycles in the positive, as well as in the negative x-direction were performed at a speed of v$=2$mm/min. Afterward, the measuring in the same direction at this shear-level was executed. Analogous, these steps (two preconditioning- and one measuring cycles) were performed in the y-direction. After finishing the stage at 50% amount of shear in both directions, a relaxation test (steptest) was conducted to investigate the visco-elastic properties of the tissue. Here, the material was sheared very quickly to a peak value of 50% (only performed for this level) and held for about 300 seconds. As always, the step test was performed in both directions. Before finishing the triaxial shear test of a single cube a compression test was performed, where the specimen was compressed to a certain value of its initial height (in our case 30%). As

already mentioned, it was necessary to test the tissue in all possible modes to get as much mechanical information as possible. The best way to obtain the information of the tissue would be to perform all six modes at a single cube. Because it was not possible with our apparatus to execute all modes at once, we cut three cubes, which lay side by side and perform two shear modes with each cube. To minimize statistical errors, a second shear test of the tissue at an other position should be conducted.

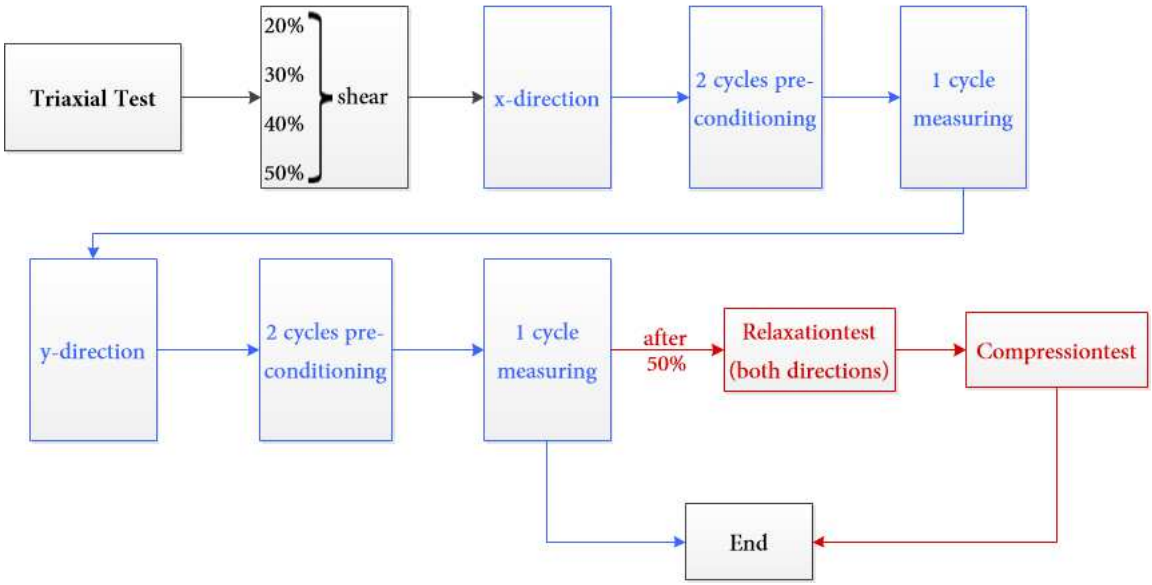

Figure 2.13.: Flow-chart showing the sequence of a complete triaxial shear test. The blue colored part of the diagram is conducted at each level of shear ones. The red part is just performed at the end of the 50% shear test.

2.3.3. Theoretical Background

The triaxial shear test relies on the mechanical theory of simple shear. More precisely this means if a cube-shaped element is sheared in one direction (in our case x- and y-direction), and the deformation gradient in 2-D becomes

$$\mathbf{F} = \begin{bmatrix} 1 & \gamma & 0 \\ 0 & 1 & 0 \\ 0 & 0 & 1 \end{bmatrix} \tag{2.9}$$

where γ is the shear strain. The shear strain can be calculated form the shear angle (Fig. 2.14).

Hence the mathematical notation for the amount of shear is

$$\tan(\phi) = \frac{\Delta x}{l} = \gamma \tag{2.10}$$

for tough materials and small angles a simplification leads to

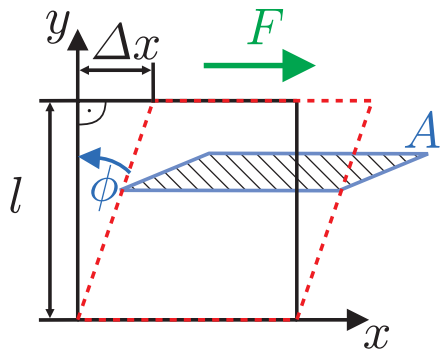

Figure 2.14.: Schematic description of simple shear, where the force F acts on a square resulting in an amount of shear γ. F..force, ϕ..shear angle, A.. cross sectional area, Δx..sheared distance in x-direction, l..length of cube in y-direction, **black**..initial state and **red**..sheared object

$$\tan(\phi) \approx \phi \tag{2.11}$$

but this is not valid for smooth biological tissue. A force (F) acting on the upper edge of a cube in the horizontal direction, like in Fig. 2.14, affects a shear stress within the body. The previously entered geometrical data of the cube is now used to calculate the shear stress τ.

$$\tau = \frac{F}{A} \tag{2.12}$$

A single shear test includes a loading path into positive, followed by a loading path into the negative direction and finally an unload until the shear strain becomes zero again. Resulting from this loading-unloading process was a specific diagram showing the form of a hysteresis, whereas the area between the two curves denotes the amount of energy that was lost during the shearing process.

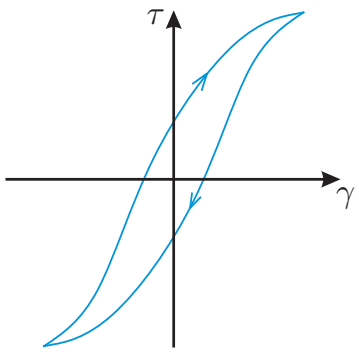

Figure 2.15.: Hysteresis that develops during a triaxial shear test. The area between the two curves represents the energy dissipation.

2.4. Multi-Photon-Microscopy Investigation

To analyze the structure of a biological tissue there are several types of investigations that can be used, e.g. magnetic resonance imaging, or histological investigation of slides etc. Due to failure of the magnetic resonance imaging and the large effort for a histological technique, we decided to perform a structural analysis with the MPM.

2.4.1. Preparation

In order to conduct such a structure analysis using MPM the specimen has to be fixated with formaldehyde solution 4% for about twelve hours. Thereafter MPM measurements can be performed. In our first attempt without performing any other preparation than the fixation, we found that the results were not satisfying concerning the penetration depth. To increase the depth of investigation as well as the quality of the gained information of the tissue, an optical-clearing was performed. Fundamentally, this process involved several preparation steps whereby the water within the tissue is substituted by a fluid with a similar index of refraction as collagen fibers (this process was an assimilation of the refraction indices of the inter- and extracellular space of the tissue). After these stages, the results were more demonstrative than before, hence the effort paid off. Moreover, an elevated measuring in depth was observed. The optical clearing encompassed three main steps: (1) Fixation (already conducted at the beginning of preparation for MPM), (2) Dehydration and (3) Clearing. Dehydration of the tissue was achieved by an increasing alcohol-sequence at 50%, 70% and 95% alcoholic strength each stage for a time of approximately 45 minutes. To finish this step, the specimen has to be laid into alcohol of 100% strength for another 90 minutes. Dehydration of the tissue must be performed because the solution used for the clearing was not soluble within aqueous compounds. Afterward, the clearing was performed by using BABB, a mixture of the two substances benzylalcohol and benzyl benzoate at a ratio of $1{:}2$. More precisely, the sample has to stay in an $1{:}1$ composition of 100% ethanol and BABB for the next four hours. Subsequently, it must be deposited into the BABB solution for at least six hours. Finalization of these steps yield to a specimen that is almost transparent, even for the human eye. The comparison of an uncleared specimen and a cleared one is shown in Fig. 2.16.

2.4.2. Measuring Theory

In general, it is sought to illustrate the most significant substances within the human adipose tissue, the collagen type I and IV. These types of proteins are not only used in the membrane of a single lipid cell but also involved at the creation of the interlobular septa. A good method to visualize these fibers is the use of MPM. MPM is a fluorescence process where a fluorophore (physical system where fluorescence appear) is excited by the simultaneous absorption of two laser photons at a certain wavelength. Second-harmonic generation (SHG) is the nonlinear optical effect which uses laser light passing through the observed tissue at a certain frequency to activate it. This technique can only be applied on biomaterials with a non-centrosymmetric molecular structure i.e. collagen. The discov-

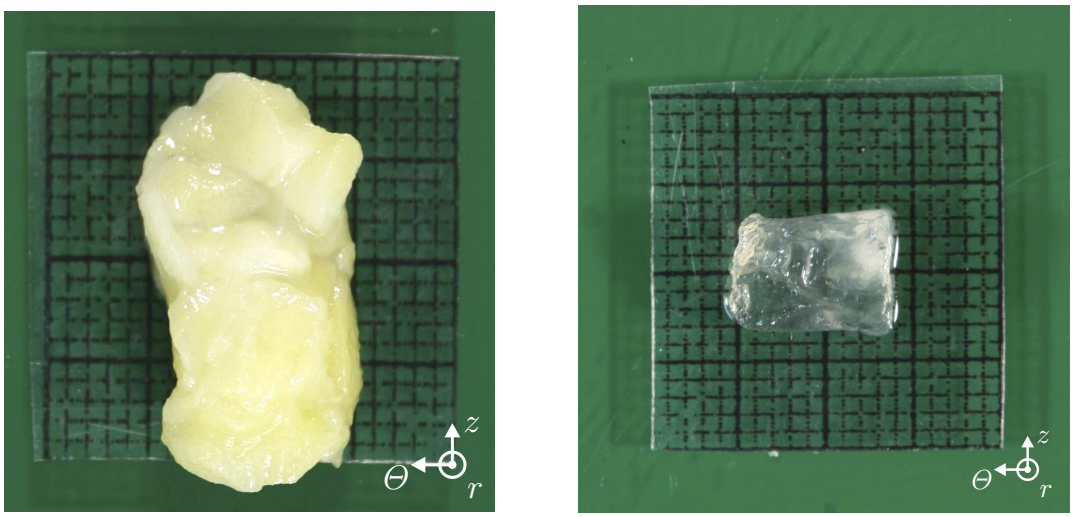

(a) (b)

Figure 2.16.: These pictures show the difference between the uncleared (a) specimen compared to the optically cleared (b) one. It is almost possible to look through the sample after the clearing process.

ered material is passed by the laser light and the photons interact with the collagen within the adipose tissue. The photons are firmly connected to the material to form new photons with twice the energy tantamount to twice the frequency as well as half the wavelength of the entering photons. In Figs. 2.17a and 2.17b one can clearly see a noticeable difference between the MPM image of an uncleared and a cleared specimen of human adipose tissue. The intercellular space of the cleared sample on the right side (Fig. 2.17b) is not fluorescent whereas the internal of the uncleared specimen is highly fluorescing. One major disadvantage is that the observed section using MPM has just a size of $620 \times 620 \mu$m. Hence, to investigate an $8 \times 8 \times 8$ cube that was investigated in the triaxial shear test, the cube has to be reassembled with many single images (this was not conducted during this project). The maximum depth of the SHG imaging is 1.5 mm. At a larger depth the absorption of the delivered photon by the surrounding tissue is too big to get good qualitative images. The schematic description in Fig. 2.18 shows the main parts of the SHG technique. By using this technique it is very easy to get a 3-D image stack of the micro-structure of the adipose tissue. If the step size between each image is chosen to be 1μm (2-D image of the certain depth of the tissue), thus a whole cube requires about 1400 to 1500 stacks.

2.4.3. Angle of Interlobular Septa

By using the software Amira, Vers. 5.3.3 by Visage Imaging Inc., we were able to measure the angles of these fibers within the human body. The graphical explanation of the two measured angles (ϕ and ψ) of the interlobular septa within the human body is demonstrated in Fig. 2.19. For performing an easy measuring the angle ϕ is defined between the z-axis and the projection of the orientation vector (ils) of the interlobular septa onto the

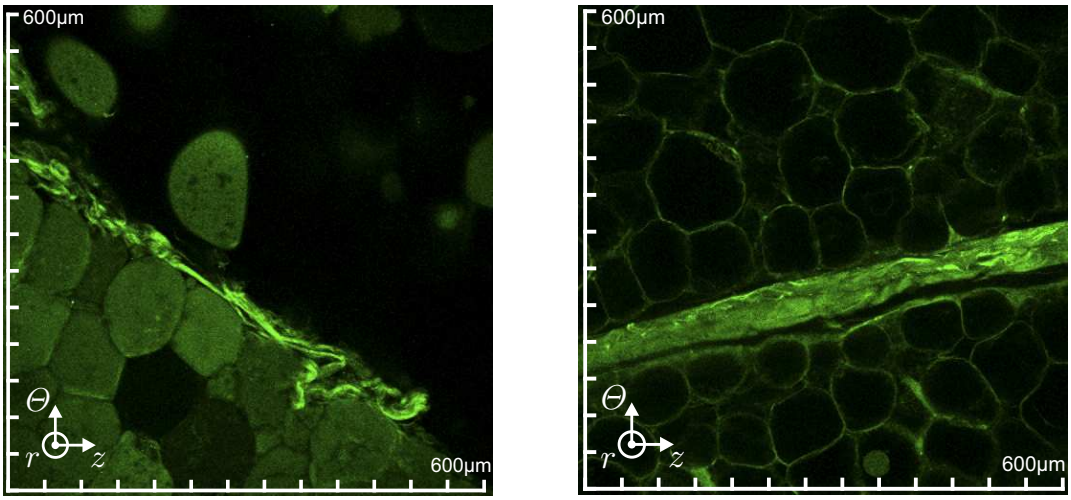

(a) (b)

Figure 2.17.: The comparison between the uncleared (a) and the cleared (b) MPM image shows that collagen fibers are emphasized and the intracellular space is not illuminating anymore. This is because of the extinction of the water within the cell.

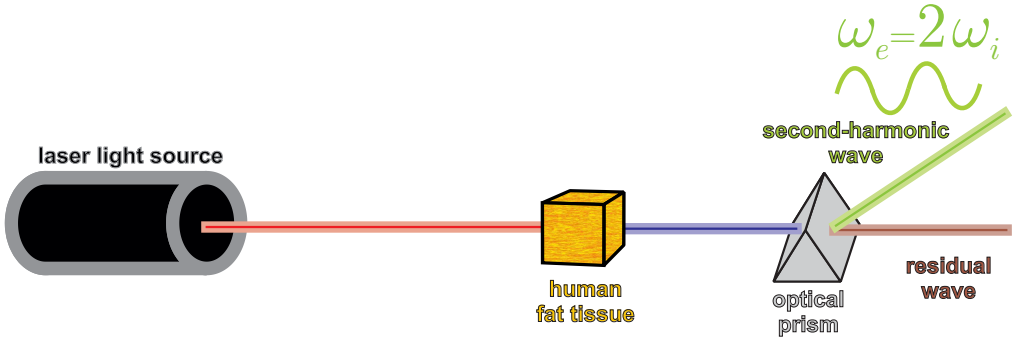

Figure 2.18.: The schematic description shows the origin photon wave (red), the residual wave (purple) and the second-harmonic wave (green) which has twice of the base frequency.

$z\theta$-plane (green arrow). The angle between the r-axis and the projection of the vector of the interlobular septa onto the $r\theta$-plane (blue arrow) is called ψ. These two angles are the most easiest to measure. Additionally to complete a description in spherical coordinates, we calculated the second angle of the spherical description ϑ (the first angle is ψ). Performing some angular calculation in the picture using the two measured values (ϕ and ψ) leads to the second angle ϑ of the spherical description.

$$\vartheta = \arctan\left(\frac{\tan(\phi)}{\sin(\psi)}\right). \tag{2.13}$$

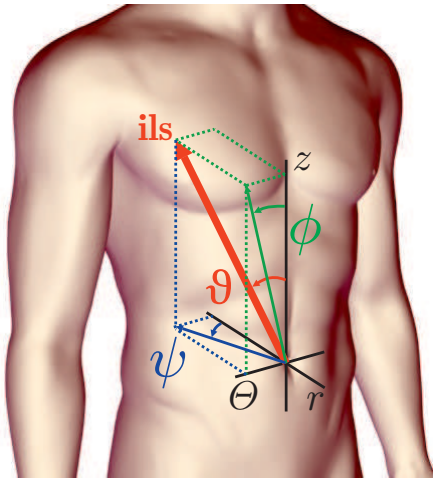

Figure 2.19.: Definition of the angles within the human body (image adopted from http://knightmare3d.webs.com/photos/Medical-Animation/).The red vector ils shows the direction of the interlobular septa within the human body. The angles ϕ and ψ were measured out of the images generate in Amira and describe the direction. The angle ϑ is a calculated value for a better imagination, because most of the people are familiar with spherical coordinates. Furthermore, there are R..Radius, h..height in z-direction and x..distance in θ-direction for calculating the second angle for the spherical coordinates.

2.5. Statistical Analysis

To proof whether the data is normal distributed a Student's t test as well as an Anderson-Darling test was used. The significance level for correlation of data was chosen to be p$= 0.05$.

3. Results

3.1. Biaxial Tension Test

In this section the results of the biaxial tensile tests of the human adipose tissue are summarized. The biaxial tensile part of the research included 18 tests of specimens from 13 different donators. Nearly all of the samples were investigated in the θz-plane, and just a single fat sample's geometry made it feasible to conduct a test in the rz-plane. In Fig. 3.2 one can see a representative diagram that shows the four quasi-static (QS), equi-biaxial cycles at the different stretch values from λ=1.05 to 1.20 in 0.05 steps. Furthermore, the non-linearity and the anisotropy of the tissue are demonstrated very well. Figure 3.3 shows the stress-strain correlation of the adipose tissue at the strain level λ=1.20 for all different ratios (1:1, 1:0.75, 0.75:1, 1:0.5 and 0.5:1). Additionally, a dynamic test at higher speed was also conducted. Due to representation problems no diagrams are shown however, the results of the dynamic test were compared to the those of the QS test. The analysis has shown that the results did not go along in normal distribution. Due to this fact, all results of the biaxial tension are plotted in a box and whiskers plot, see e.g. the box plot for dynamic and quasi-static tension at 15% stretch in Fig.3.1. By reason of bad comparison characteristics of the median, the mean value and the standard deviation (SD) were also calculated. Moreover, these value were just used to show a trend rather than performing detailed comparison of numerical values. To see all other box plots the reader is referred to the appendix. Table 3.1 lists the results (mean and SD) of the normal stress for the dynamic and the normal biaxial tension test.

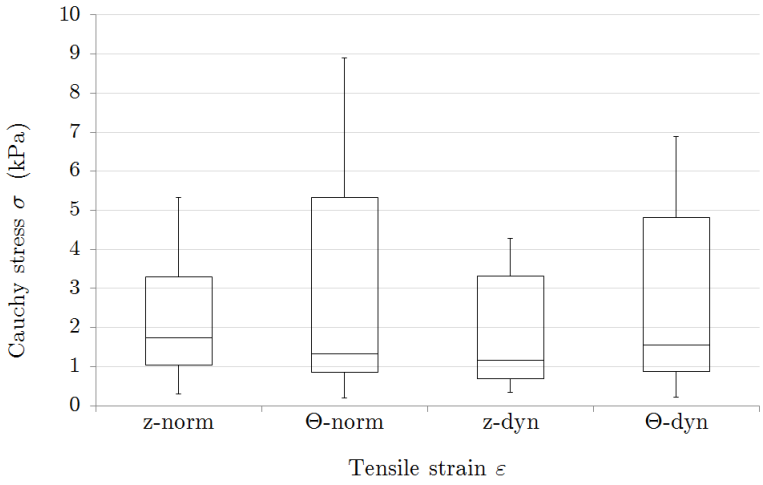

Figure 3.1.: Diagram of the not normal distributed data of the biaxial tension test. Showing the data for dynamic and quasi-static test at 15% stretch.

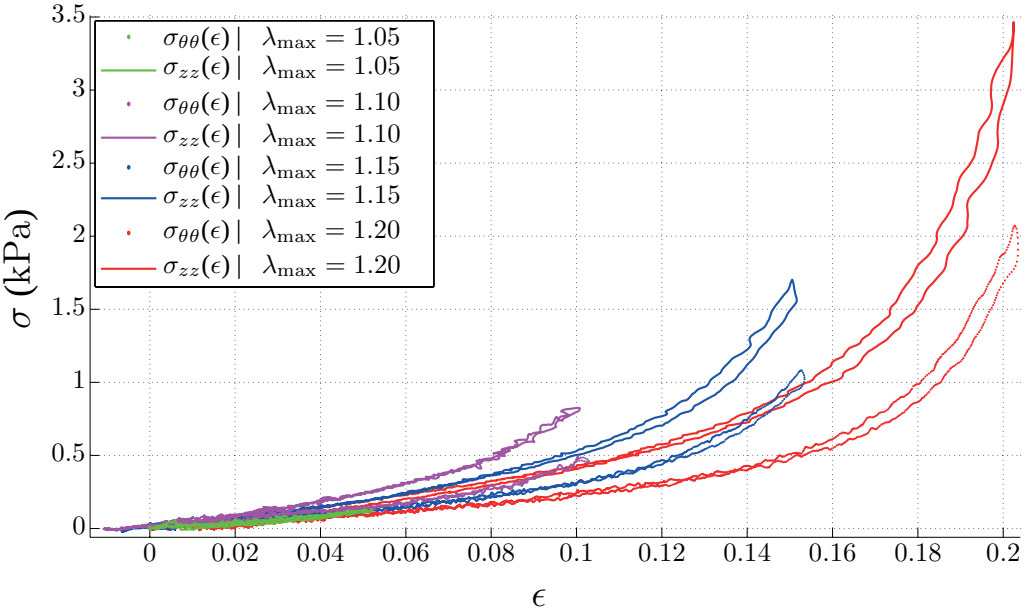

Figure 3.2.: Representative equi-biaxial stress-stretch behavior of human abdominal adipose tissue from 5% to 20% stretch in 5% steps. The anisotropic as well as the non-linear behavior is clearly visible.

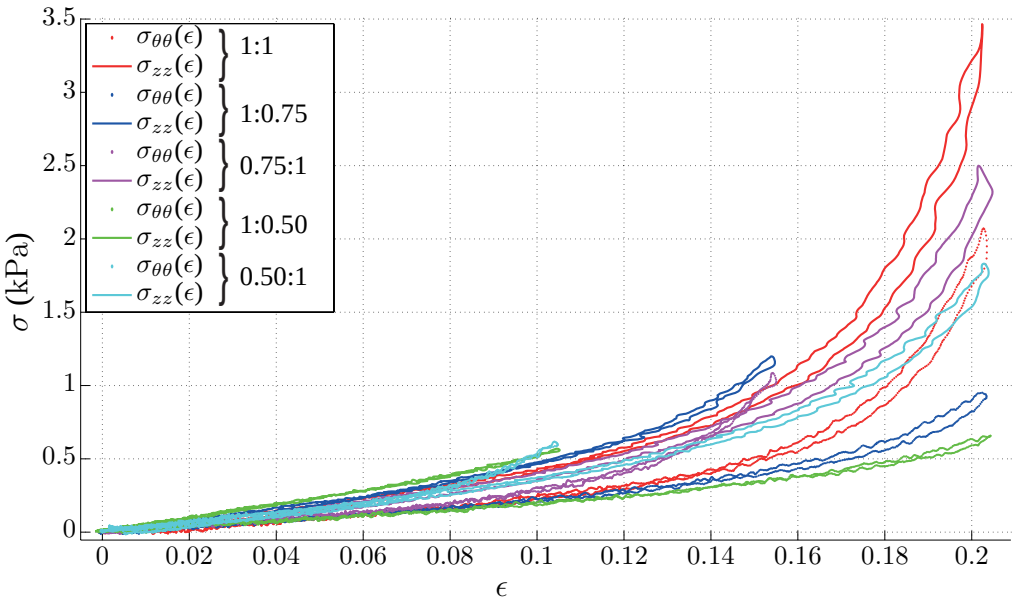

Figure 3.3.: Cauchy stress versus strain during a biaxial stretch test for 20% stretch at different ratios.

Table 3.1.: The mean values and the standard deviation (SD) of the normal stress for all three directions both for the normal and dynamic biaxial tension tests are shown. n..normal mode, d..dynamic mode.

		longitudinal		transversal		sagittal	
Strain	Mode	MEAN kPa	SD kPa	MEAN kPa	SD kPa	MEAN kPa	SD kPa
0.05	n	0.52	0.59	0.45	0.46	0.14	0.14
	d	0.65	0.58	0.46	0.33	0.46	-
0.10	n	0.90	0.78	0.51	0.28	0.35	0.35
	d	0.54	0.38	0.62	0.54	0.62	-
0.15	n	1.82	1.44	2.69	2.88	0.71	0.71
	d	1.50	1.29	2.24	2.14	2.24	-
0.20	n	3.42	2.12	4.01	3.47	-	-
	d	2.98	2.47	3.07	2.13	-	-

3.1.1. Quasi-Static Test

The obtained results for the QS test (Fig 3.4), show higher amplitudes in the transversal direction, for larger stretch values (larger than 10%). At lower strain magnitudes, the longitudinal direction is stiffer, in the contrary to our expectations in the first place, although, the difference is not large. The sagittal direction appears to be the softest. The significance of this result, however, can not be taken into account seriously because only one specimen was tested in this plane.

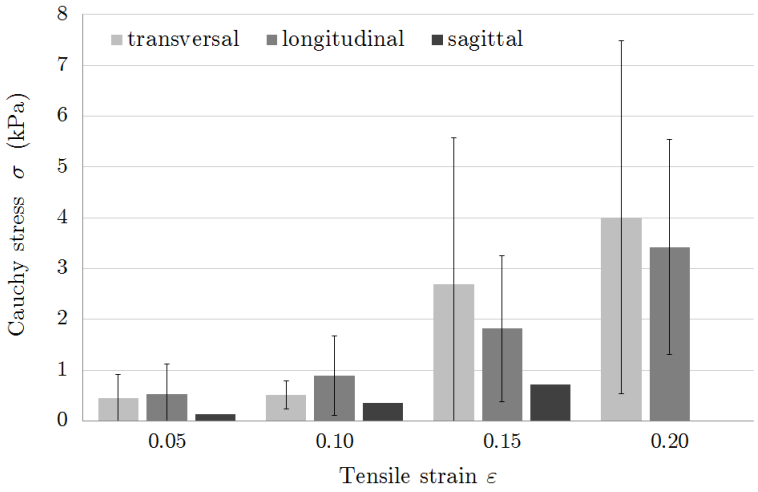

Figure 3.4.: Mean values of the stress-strain relation for the tested adipose tissue at four different stretch magnitudes. Noticeable is the change from 10%, where longitudinal direction was stiffer, to 15%, after what the transversal direction was stiffer (results from Tab. 3.1).

3.1.2. Comparison with Dynamic Test

Another interesting fact was, whether the response of the material is dependent of the strain rate (speed that is chosen to achieve the strain level divided by the initial length). Figure 3.5 shows the results of the comparison of the mean values of the normal (QS) with the dynamic test. The proportionality changes in evidence for longitudinal and transversal direction from 10% stretch to 15%, respectively. The sagittal direction behaves stiffer for QS tension at 5%, almost equally stiff for both modes at 10% and in the end stiffer at the dynamic tension at 15% stretch.

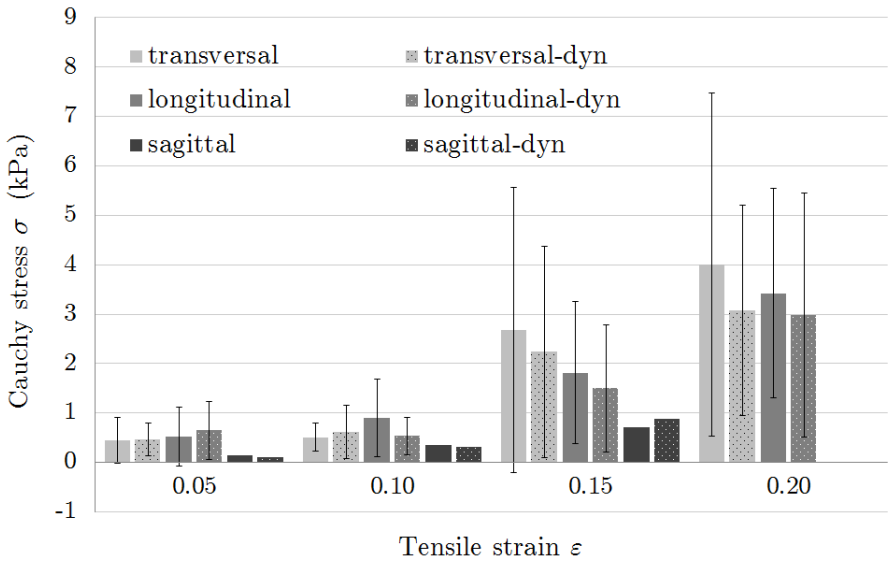

Figure 3.5.: Mean values of the stress-strain relation of dynamic and QS mode. The transversal direction becomes stiffer at the QS test compared to the dynamic test at 10% stretch although, it is softer for 5% stretch . Same change of amplitudes can be observed in longitudinal direction for 15% stretch whereby, the material is slightly stiffer in dynamic test in the previous two phases. The sagittal direction also changes the proportionality of QS to dynamic for high stretch.

3.2. Triaxial Shear Test

The test software package is able to export several values of the triaxial shear apparatus. In our case we exported the shear-stresses, which was already calculated, the shear-strain in x- as well as in y-direction for the shear measure and the step-test, plus the stress values in z-direction for the compression test to be written into a file (directions are written in coordinates of the apparatus). Additionally, for calculating the volume of the specimen and furthermore the dissipated energy, we exported the geometry of the specimen. Due to the slow testing speed, the noise portion is not negligible. This means that the usage of a noise filter is essential. This is realized during the preprocessing of the obtained data, before using it for further analysis. Figure 3.6 shows both, the noise on the curve and the smoothed curve.

The specimen of 16 different donators were investigated with the triaxial shear test apparatus. Because we tried to perform two complete tests (six specimen necessary) on each fat sample, we got a total amount of 24 results. The four significant curves for loading and unloading cycle, of a shear test, with its typical hysteresis characteristic, at all amounts of shear of (20%, 30%, 40% and 50%) are shown for $r\theta$- and rz-mode in Fig. 3.7, for θz- and θr-mode in Fig. 3.8 and for zr- and $z\theta$-mode in Fig. 3.9. The results show a

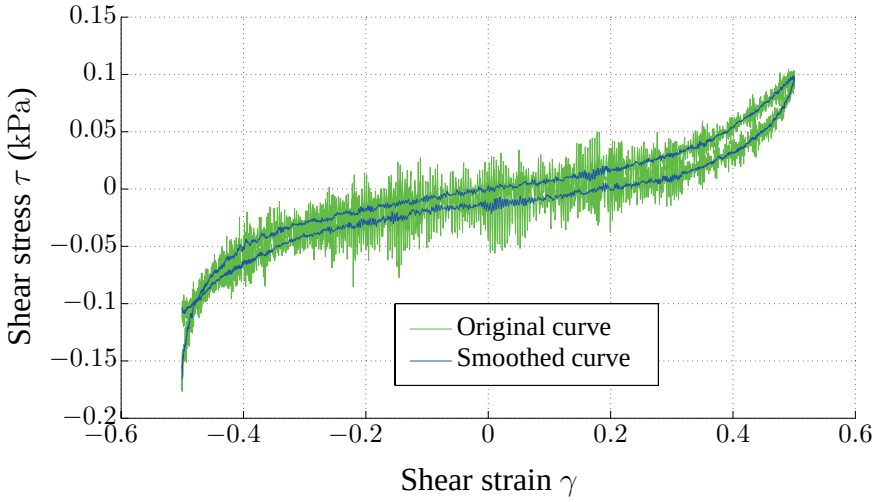

Figure 3.6.: In green the original curve with noise included; in the front with blue color is the mean curve which is already smooth.

slight difference in the magnitudes of the stress in positive and negative direction. The curve for the relaxation test in all three directions and the compression test is showed in Figs. 3.10, 3.11, 3.12 and 3.13, respectively.

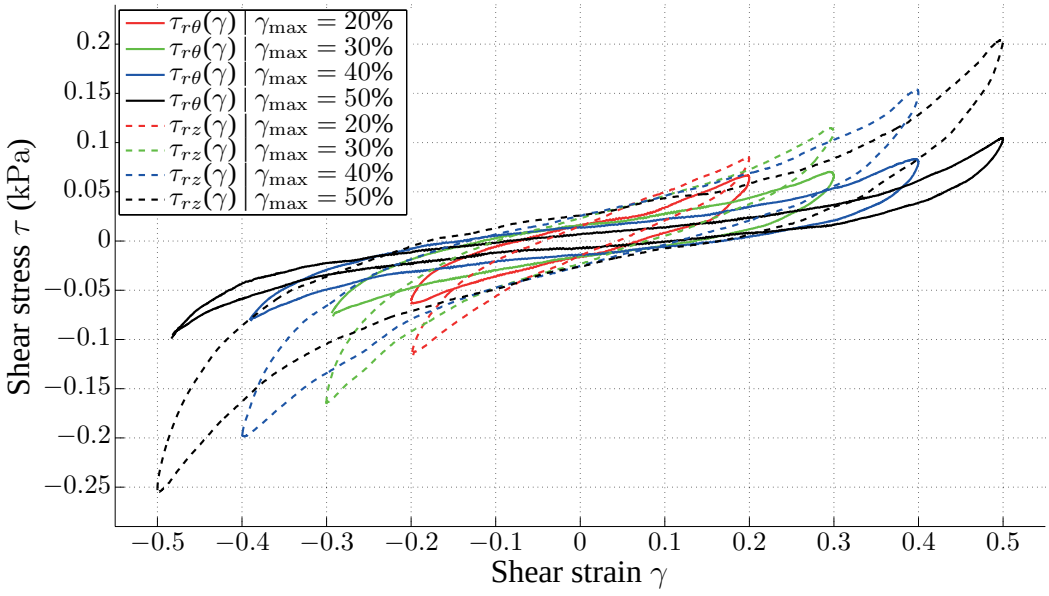

Figure 3.7.: Representative shear stress vs. strain (amount of shear) behavior of a complete triaxial test in $r\theta$- and rz-direction including shearing in positive and negative direction at levels of 20%, 30%, 40% and 50% shear.

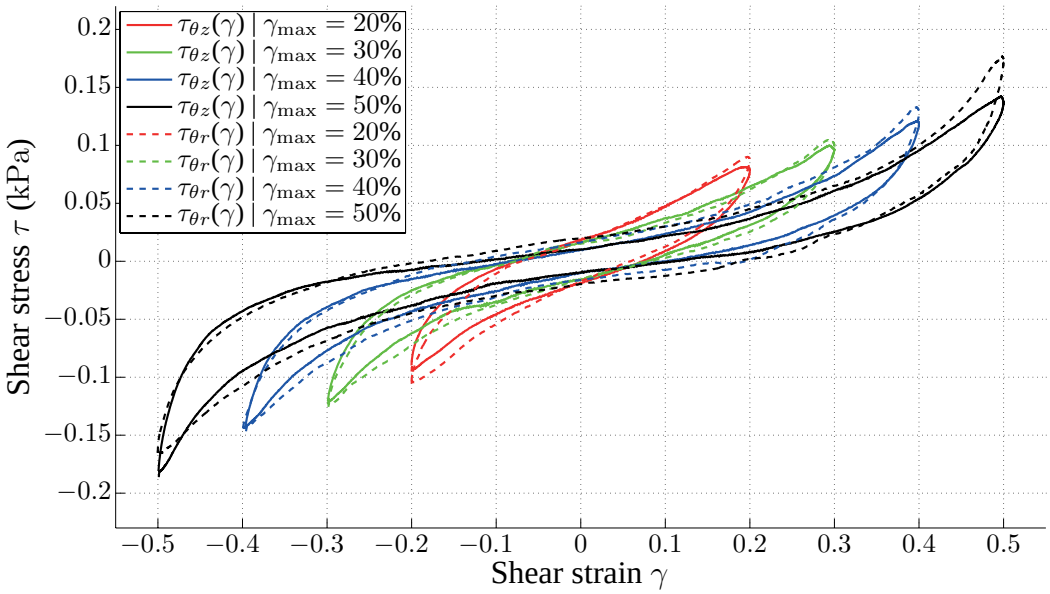

Figure 3.8.: Representative shear stress vs. strain (amount of shear) behavior of a complete triaxial test in θz- and θr-direction including shearing in positive and negative direction at levels of 20%, 30%, 40% and 50% shear.

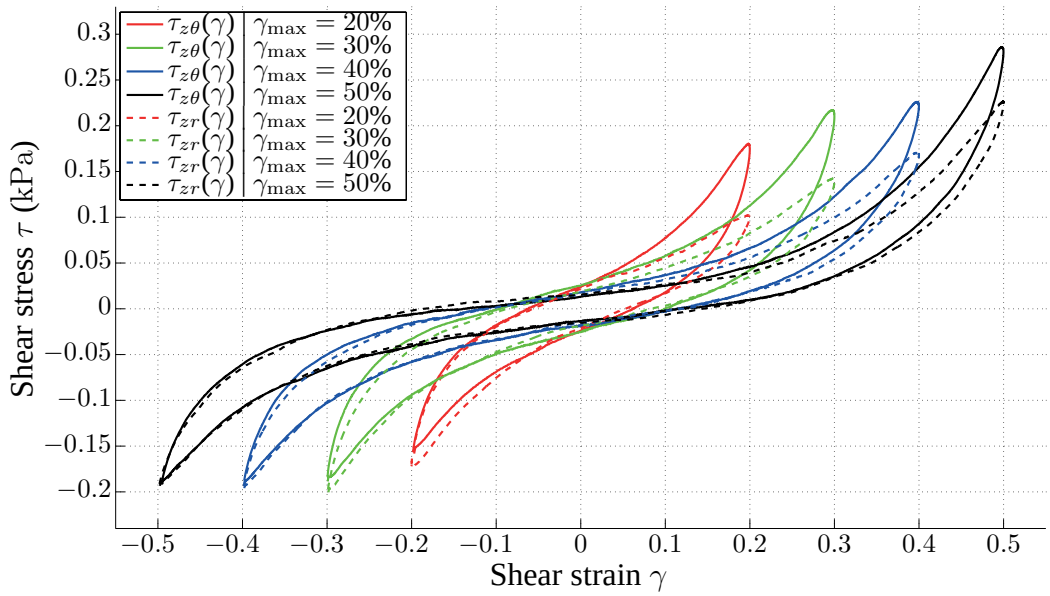

Figure 3.9.: Representative shear stress vs. strain (amount of shear) behavior of a complete triaxial test in zr- and $z\theta$-direction including shearing in positive and negative direction at levels of 20%, 30%, 40% and 50% shear.

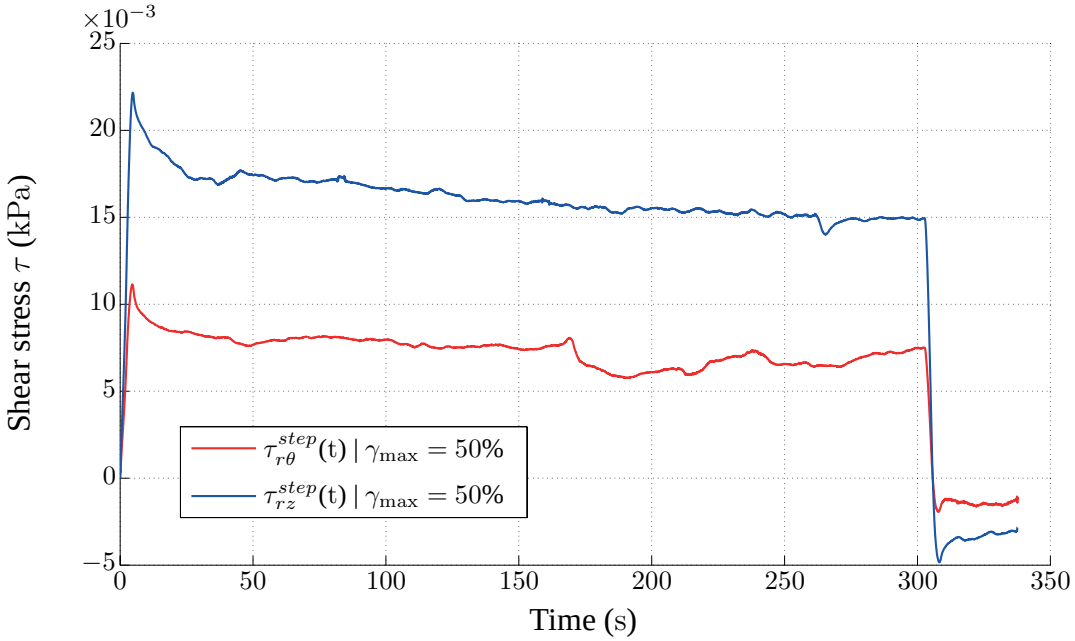

Figure 3.10.: The steptest in $r\theta$- and rz-direction up to a maximum amount of shear $\gamma_{\max}$=50%.

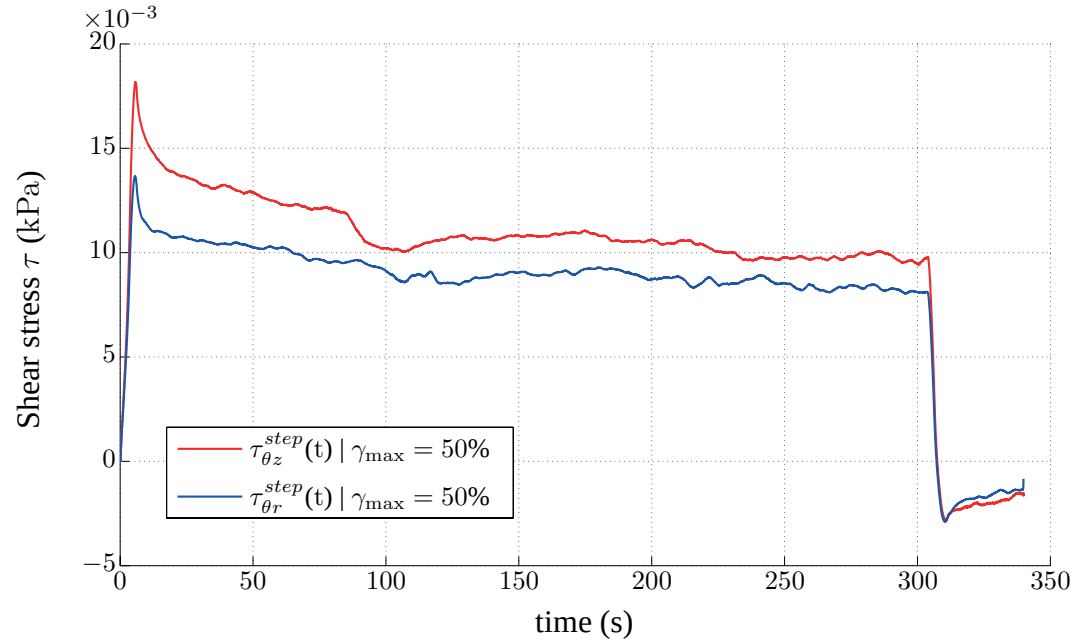

Figure 3.11.: The steptest in θz- and θr-direction up to a maximum amount of shear $\gamma_{\max}$=50%.

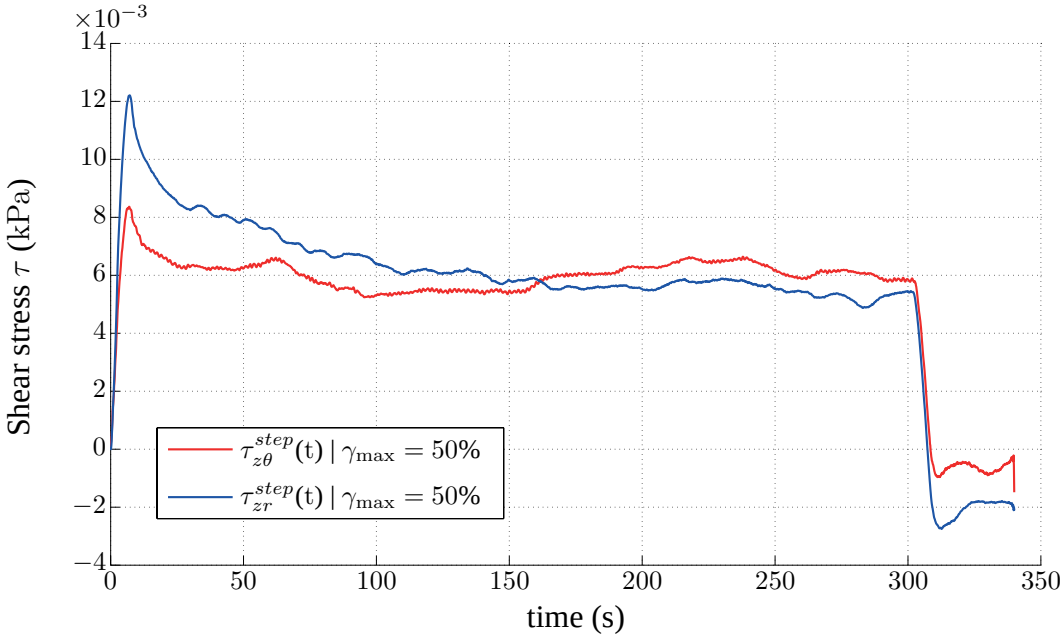

Figure 3.12.: The steptest in zr- and $z\theta$-direction up to a maximum amount of shear $\gamma_{\max}$=50%.

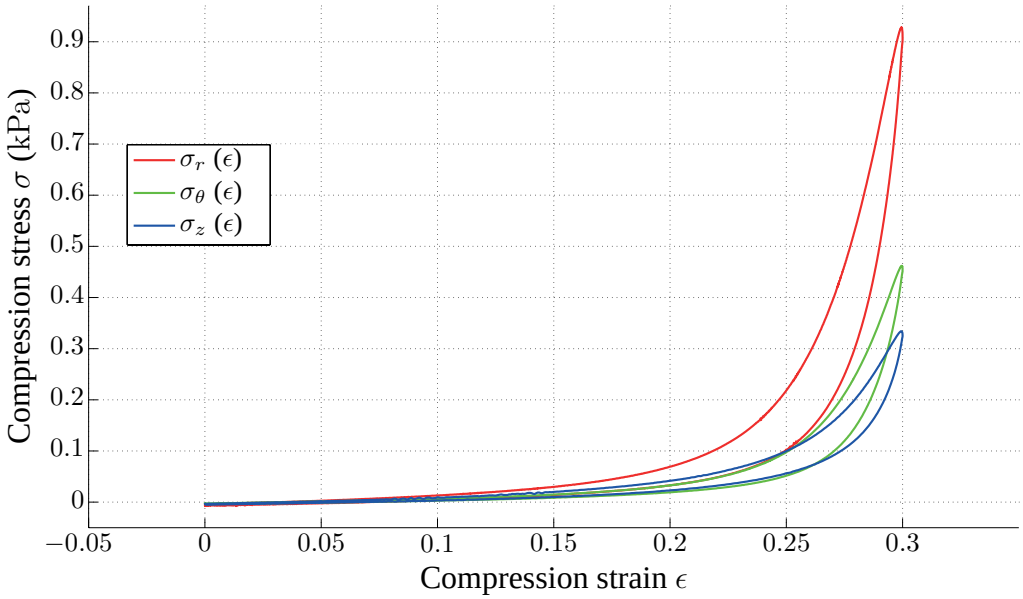

Figure 3.13.: Compression test is performed at the end of the triaxial shear test. Here a shortening of 30% of the specimens height was conducted.

3.2.1. Shear Test

During the shear test, a maximal and minimal amplitude of the stress, due to the shearing in both directions, can be measured (Tab. 3.2). In our opinion, it makes sense to analyze the magnitude in both the positive and the negative direction as well as calculating a mean value of the absolute values, by reason of minimization of an occurring error. Results from Tab. 3.4 are visualized separately in the respective subsection.

Table 3.2.: Mean values and standard deviation (SD) of the shear stress for all shear modes and strains in positive and negative direction as well as the mean of both.

Mode	Shear amount	MEAN_{pos} kPa	SD_{pos} kPa	MEAN_{neg} kPa	SD_{neg} kPa	$\text{MEAN}_{\text{mean}}$ kPa	SD_{mean} kPa
zr	20 %	0.051	0.025	-0.067	0.040	0.059	0.033
	30 %	0.056	0.021	-0.088	0.047	0.072	0.034
	40 %	0.094	0.052	-0.127	0.074	0.110	0.063
	50 %	0.129	0.072	-0.150	0.078	0.140	0.075
$z\theta$	20 %	0.047	0.015	-0.072	0.047	0.059	0.031
	30 %	0.055	0.017	-0.112	0.088	0.084	0.052
	40 %	0.096	0.054	-0.208	0.197	0.152	0.125
	50 %	0.119	0.062	-0.267	0.259	0.193	0.160
θr	20 %	0.067	0.041	-0.100	0.060	0.083	0.050
	30 %	0.082	0.048	-0.115	0.061	0.099	0.054
	40 %	0.126	0.081	-0.159	0.088	0.142	0.085
	50 %	0.146	0.091	-0.218	0.126	0.182	0.109
θz	20 %	0.072	0.041	-0.086	0.038	0.079	0.040
	30 %	0.095	0.050	-0.117	0.050	0.106	0.050
	40 %	0.142	0.093	-0.199	0.140	0.170	0.116
	50 %	0.195	0.117	-0.228	0.128	0.211	0.122
$r\theta$	20 %	0.049	0.023	-0.064	0.027	0.057	0.025
	30 %	0.060	0.028	-0.083	0.032	0.071	0.030
	40 %	0.071	0.035	-0.095	0.048	0.083	0.041
	50 %	0.094	0.057	-0.117	0.074	0.106	0.065
rz	20 %	0.046	0.015	-0.059	0.026	0.053	0.020
	30 %	0.059	0.022	-0.069	0.029	0.064	0.026
	40 %	0.077	0.040	-0.078	0.042	0.078	0.041
	50 %	0.091	0.050	-0.110	0.062	0.100	0.056

The statistical analysis of obtained data did not show a normal distribution. Hence, the results are represented in box plots. The Fig. 3.14 is an example for a box plots for the respective test at 30% shear. To see all other box plots the reader is referred to the appendix. Nevertheless, because of a better comparison the results are presented in mean value and standard deviation (SD). The diagrams are just shown to indicate trends and not to compare numerical values.

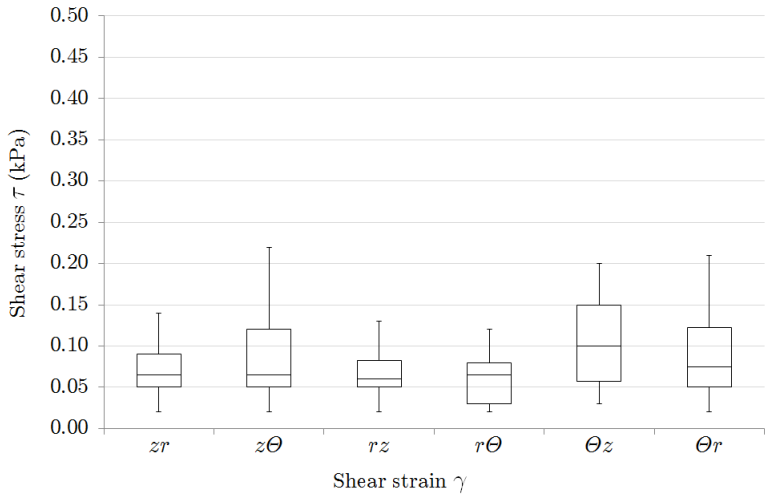

Figure 3.14.: Data for 30% shear in positive direction. Results are not normal distributed and therefore shown in box plot.

Positive Direction

Figures 3.15, 3.16, 3.17 and 3.18 show the mean values of the stress in the tissue sheared into the positive direction. The magnitudes are lower compared to the negative shear direction. Here, the maximum always occurs at the shear in θz-direction. Same as at the shearing in the negative direction the minima are always in the $r\theta$- and rz-direction.

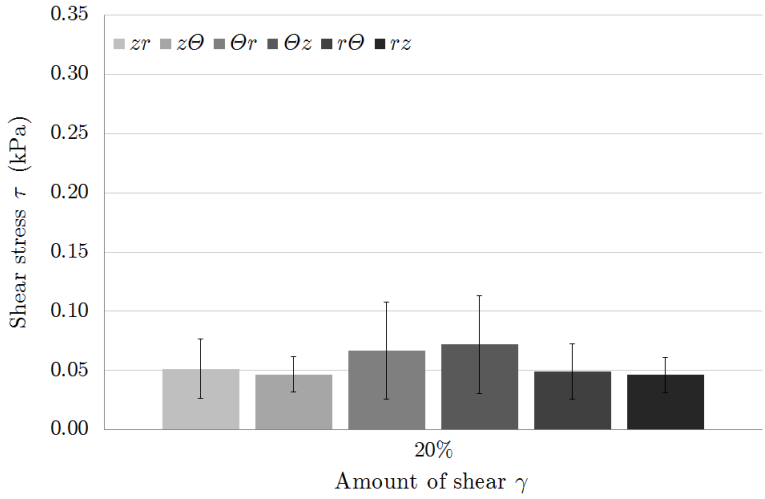

Figure 3.15.: Shear stress at 20% shear strain for all six shear modes. The stiffest direction here is the θz-direction. The magnitude is smaller compared to the stress in the negative direction.

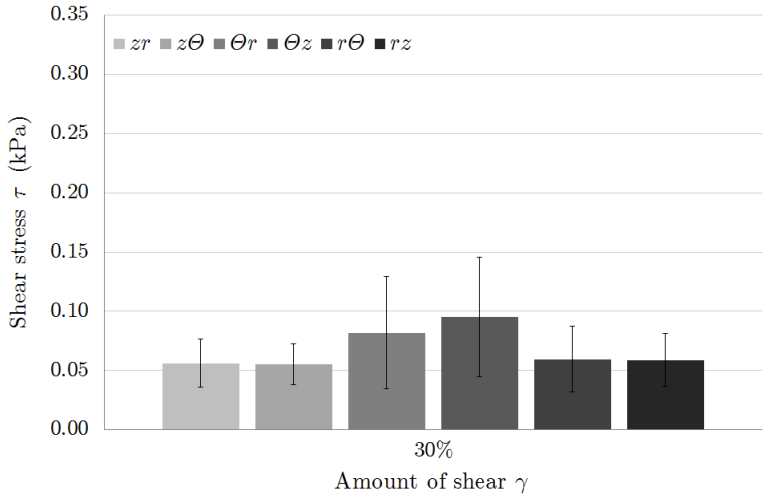

Figure 3.16.: Shear stress at 30% shear strain for all six shear modes. Again the θz-direction is the stiffest with a amplitude of approximately 0.1 kPa.

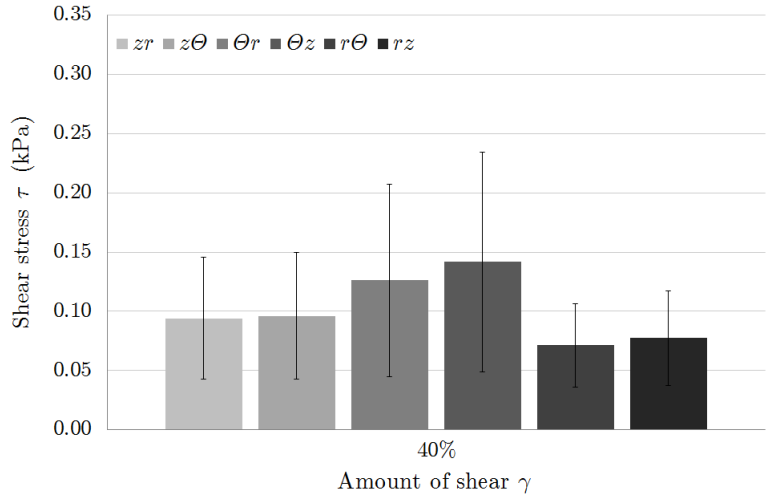

Figure 3.17.: Shear stress at 40% shear strain for all six shear modes. The maximum value reaches almost 0.15 kPa for the θz-direction.

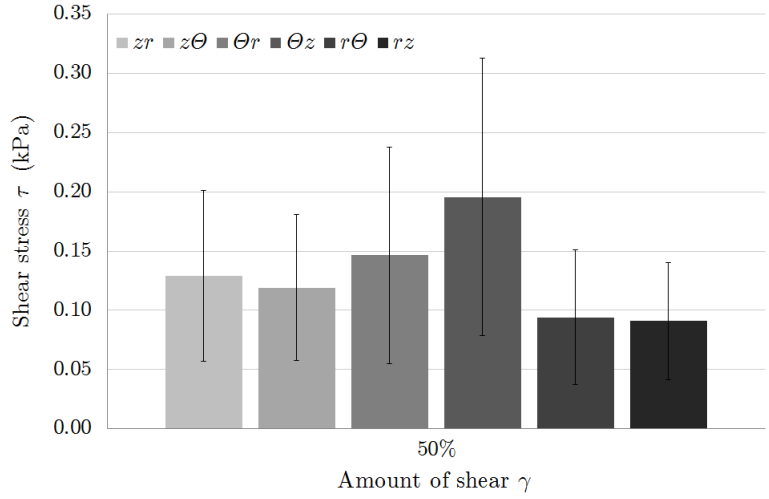

Figure 3.18.: Shear stress at 50% shear strain for all six shear modes. As before the maximum value is obtained for the θz-mode at approximately 0.35 kPa.

Negative Direction

In Figs. 3.19, 3.20, 3.21 and 3.22 the mean values of the stress in the tissue for the negative shear direction is shown. The magnitudes' dimension double from 20% to 50% shear strain. The maximum in total changes from θr- towards $z\theta$-mode, however, the minimums always appear during the $r\theta$- and rz-mode.

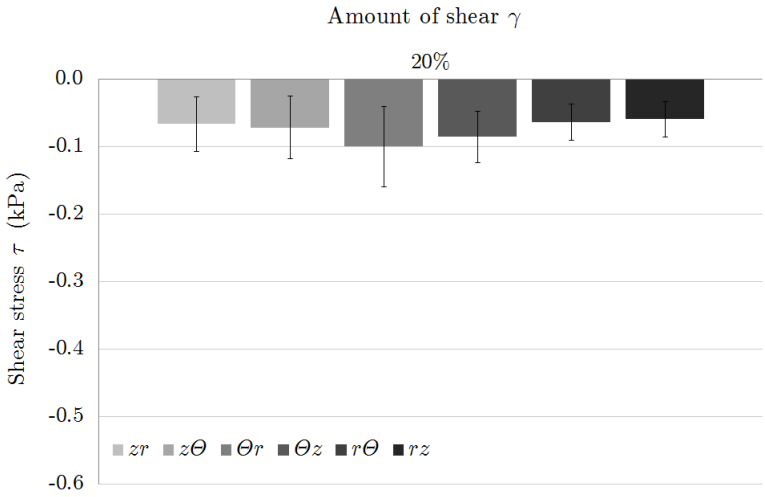

Figure 3.19.: Shear stress at 20% shear strain for all six shear modes. The stiffest direction here is the θr-direction, although the magnitude is not high.

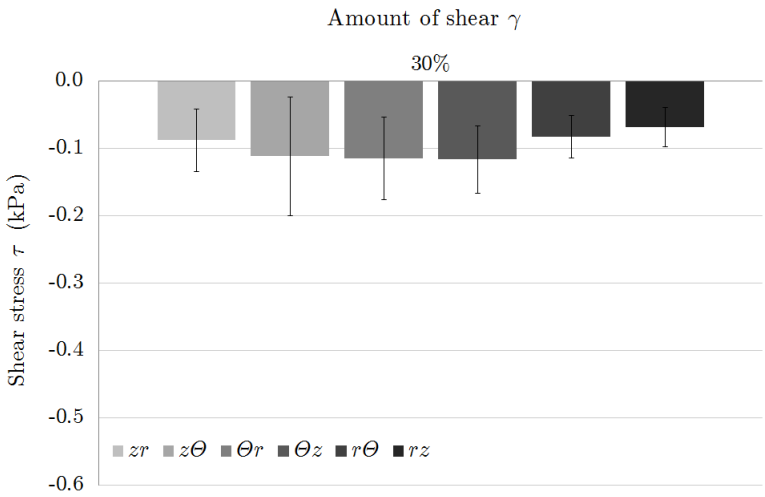

Figure 3.20.: Shear stress at 30% shear strain for all six shear modes. Tthere are three directions with almost the same amplitude of -0.1 kPa.

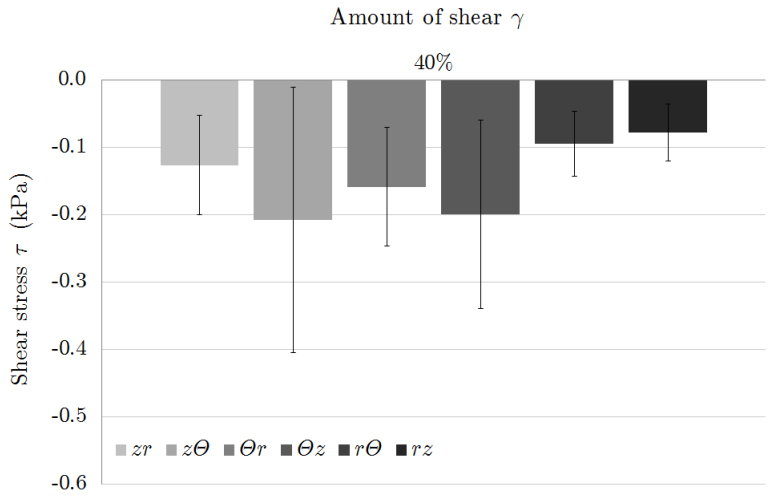

Figure 3.21.: Shear stress at 40% shear strain for all six shear modes. The maximum lies approximately at -0.2 kPa at the $z\theta$- and θz-direction.

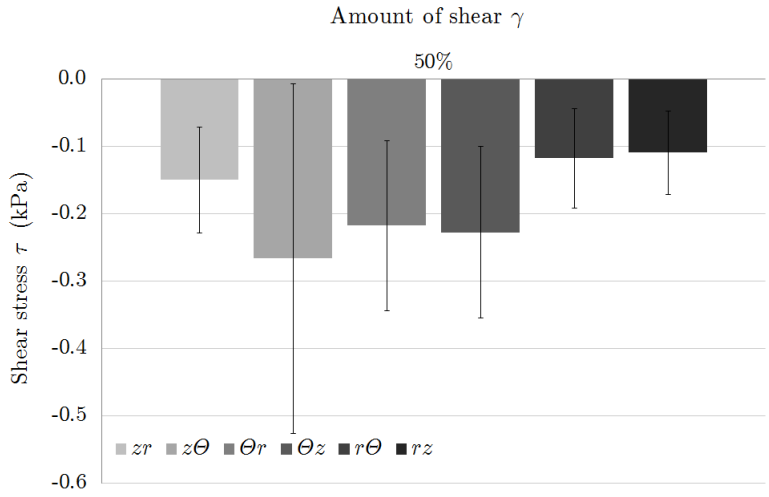

Figure 3.22.: Shear stress at 50% shear strain for all six shear modes. The stiffest direction at the highest stretch is the $z\theta$-direction with a magnitude of -0.26 kPa.

Mean Value of Both Direction

Due to the different magnitudes in positive and negative direction it is reasonable to calculate the mean value of the two results. Figures 3.23, 3.24, 3.25 and 3.25 show the mean values of the stress of both directions. For 20% amount of shear the largest magnitude occur at θr- and θz-mode. Afterwards, the magnitude in θz-direction is the largest.

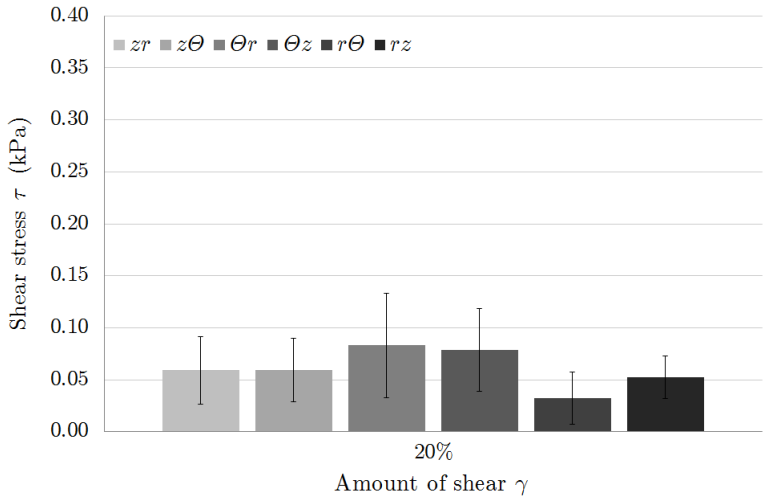

Figure 3.23.: Shear stress at 20% shear strain for all six shear modes. The stiffest direction here is the θr-direction. The magnitude reaches almost 0.1 kPa.

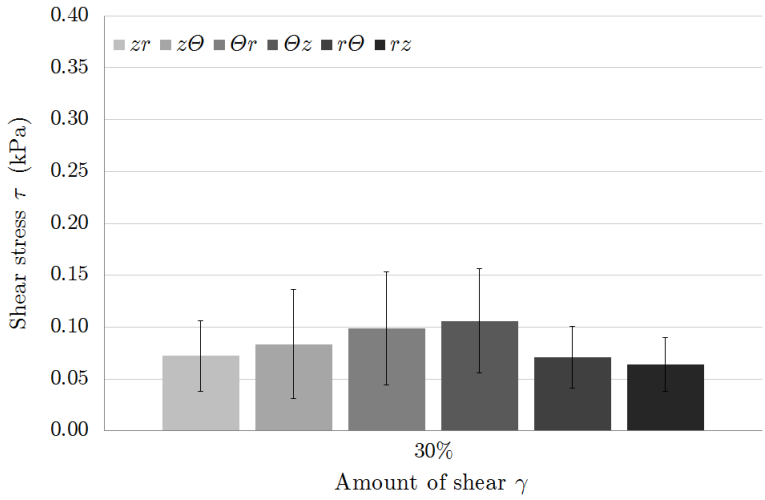

Figure 3.24.: Shear stress at 30% shear strain for all six shear modes. Here the θz-direction is the stiffest with a amplitude little bit higher than 0.1 kPa.

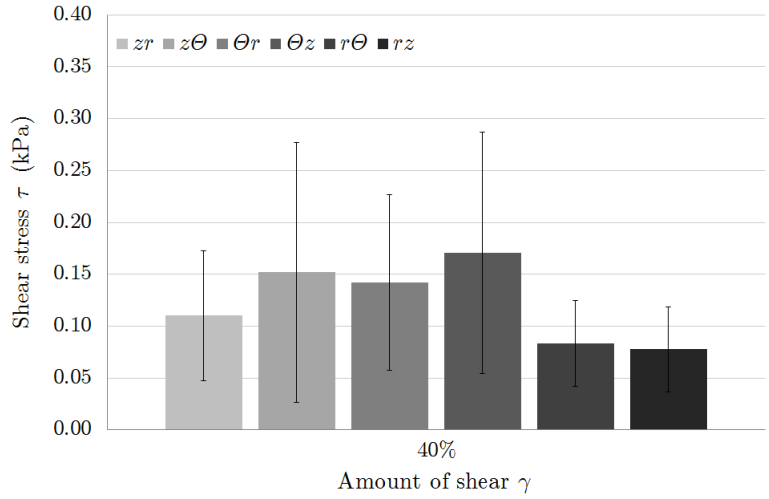

Figure 3.25.: Shear stress at 40% shear strain for all six shear modes. The magnitude exceeds the value 0.15 kPa for the θz-direction.

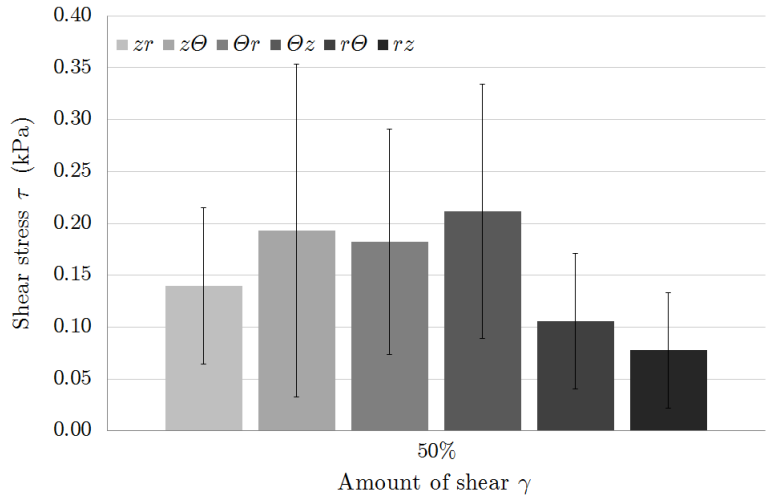

Figure 3.26.: Shear stress at 50% shear strain for all six shear modes. As it was before the maximum value is obtained for the θz-mode at approximately 0.21 kPa.

3.2.2. Relaxation Test

Another part of the triaxial shear test was the relaxation test. We decided to calculate two different parameters from the relaxation time diagrams: (i) the relaxation time ($\mathrm{t_R}$), which means the time in the relaxation diagram where the stress value has increased to 63% of the magnitude and (ii) a peak-to-plateau (PtoP) value which signifies the relation between the peak value and the constant part of the stress-time diagram, leading to a value without units. Figures 3.27 and 3.28 show the results for $\mathrm{t_R}$ and the value PtoP, respectively. Some of the results of $\mathrm{t_R}$ had to be cleaned out because the relaxation of the tissue seemed to last longer than the actual test time was. The results for the $\mathrm{t_R}$ show that the range is almost the same for all shear-modes (between 60 and 80 s). The largest values can be observed for relaxation in θz- and θr-direction. Table 3.3 shows the results for the relaxation time and the peak-to-plateau value.

Table 3.3.: Showing the mean value and standard deviation for the relaxation time($\mathrm{t_R}$) and the peak-to-plateau value (PtoP).

Mode	MEAN($\mathrm{t_R}$) s	SD($\mathrm{t_R}$) s	MEAN(PtoP) -	SD(PtoP) -
rz	62	40	1.80	0.40
$r\theta$	66	60	1.57	0.38
zr	63	40	1.65	0.33
$z\theta$	69	46	1.50	0.24
θr	71	50	1.56	0.26
θz	78	43	1.61	0.25

The lowest and the largest PtoP values were obtained at 1.5 and the largest at 1.8, respectively. The PtoP values were distributed equally for all shear-modes.

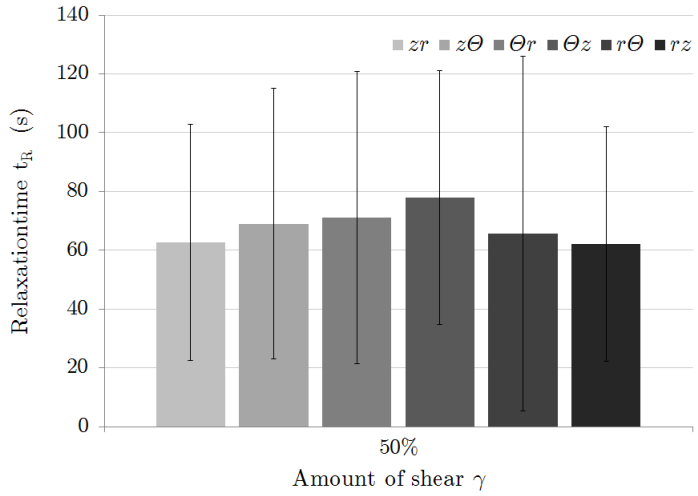

Figure 3.27.: The results to the relaxation test for the different shear-modes. The maximal time duration is observed in the θz-direction, which means that the viscosity is in this direction larger compared to the others.

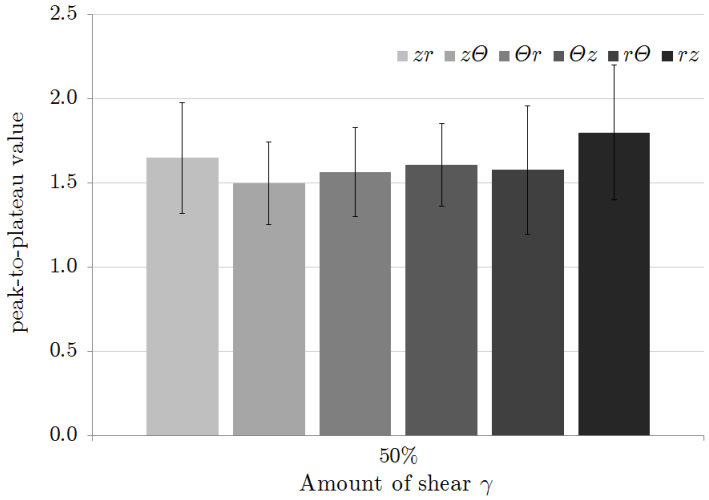

Figure 3.28.: Results from calculation of the value showing that the range of the relation of the two phases lies between 1.5 and 1.8 for all the tested modi.

3.2.3. Compression Test

The compression test was the last test before finishing the triaxial shear test. The diagram in Fig. 3.29 shows the results for the compression of the tissue in the three possible directions r, z and θ. Here, the compression in transversal direction is the stiffest, the maximum is almost twice than in the other directions. In Tab. 3.4 one can find the results for the compression stress in each direction.

Table 3.4.: Showing mean values and standard deviation (SD) of the compression stress in the three possible directions.

Mode	MEAN kPa	SD kPa
z	0.26	0.19
r	0.33	0.30
θ	0.49	0.55

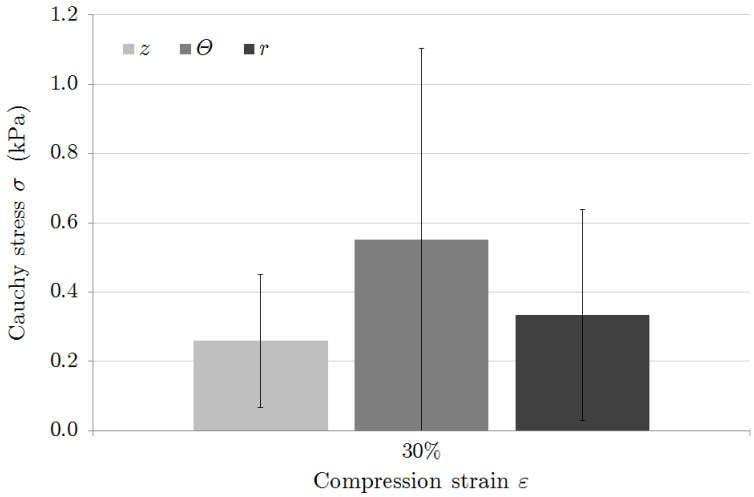

Figure 3.29.: Results from the 30% compression test in z-direction of the machine. Stiffest direction at this type of loading is the θ-direction.

3.2.4. Dissipated Energy

Another point of the analysis of the triaxial shear data is the calculation of the dissipated energy during one loading- and unloading cycle. The results of this calculation are shown in Figs. 3.30, 3.31, 3.32 and 3.33 for the different shear strains. The energy level for all shear-modes for each amount of shear (20%, 30% and 40%) range was almost at the same level. At 50% shear strain the maximum energy dissipation occurred in θz-direction, see Tab. 3.5.

Table 3.5.: Showing the mean values and the standard deviation (SD) of the dissipated energy (W_H) in all possible shear modes.

Shear	zr		$z\theta$		θr		θz		$r\theta$		rz	
strain	W_H μNm	SD μNm	W_H μNm	SD μNm	W_H μNm	SD μNm	W_H μNm	SD μNm	W_H μNm	SD μNm	W_h μNm	SD μNm
20 %	2.19	1.01	2.03	0.93	2.39	1.48	2.11	0.80	2.36	1.27	2.31	1.26
30 %	3.29	1.84	2.94	1.33	3.22	1.47	3.24	1.61	3.31	1.53	3.53	1.21
40 %	4.45	2.13	4.50	1.95	4.59	2.28	4.96	2.39	4.11	1.88	4.76	2.70
50 %	6.54	3.38	6.59	3.96	5.79	2.62	7.94	3.56	6.28	4.07	7.10	2.99

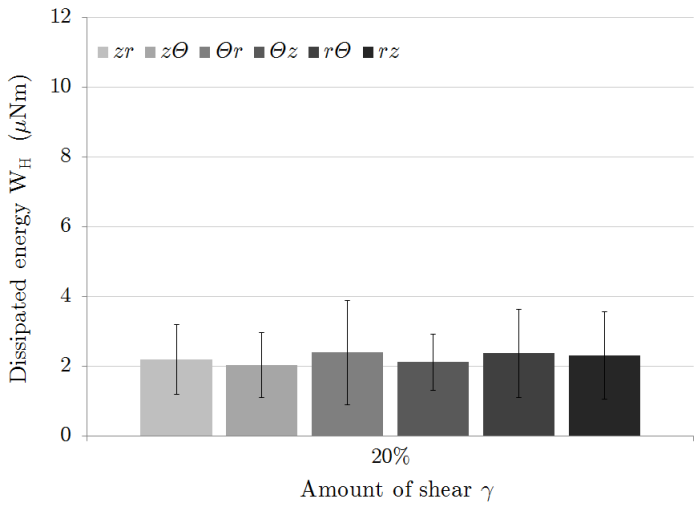

Figure 3.30.: Energy dissipation for one cylce during the shear test at 20% amount of shear for all shear-modes.

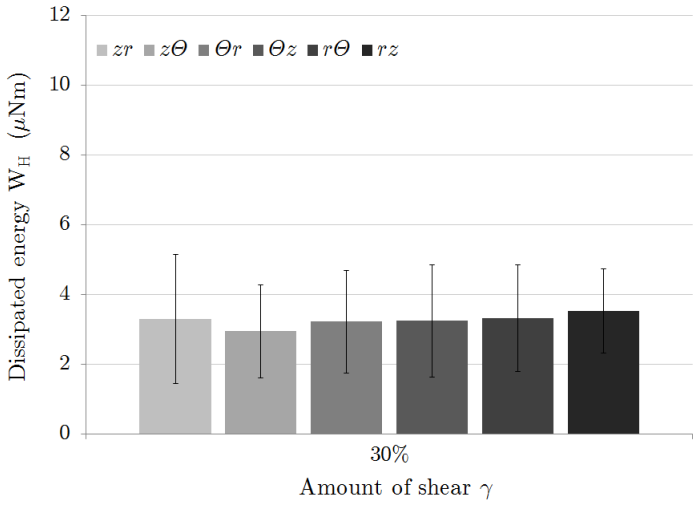

Figure 3.31.: Energy dissipation for one cycle during the shear test at 30% amount of shear for all shear-modes.

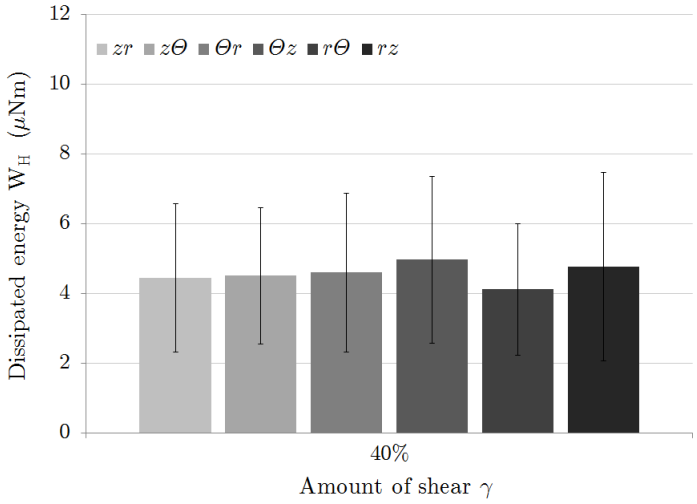

Figure 3.32.: Energy dissipation for one cycle during the shear test at 40% amount of shear for all shear-modes.

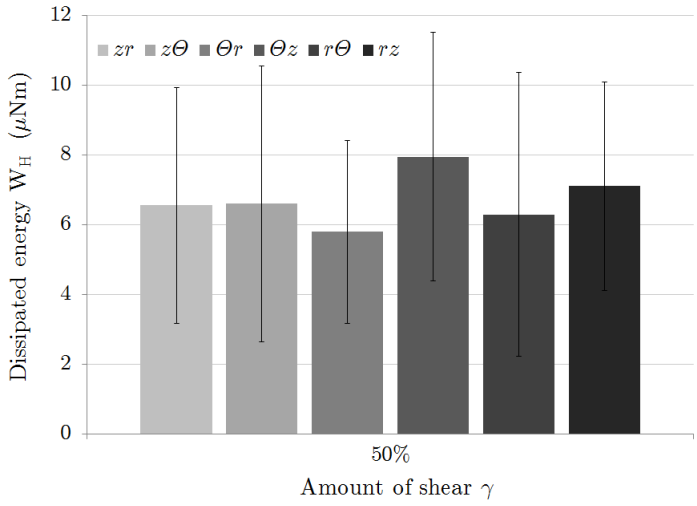

Figure 3.33.: Energy dissipation for one cycle during the shear test at 50% amount of shear for all shear-modes.

3.3. Multi-Photon-Microscopy Investigations

We prepared eight specimens from four different donators with the photo-clearing process. Previously, a measuring of a specimen was conducted without preparing the tissue. Two of the results were not useful for interpretation because of bad image qualities. More specific, one image stacks was obtained from sample no. I, one from sample no. VI and two from no. VII (because the first stack was not a good quality). The last image stake was acquired from sample no. IX.

3.3.1. Preprocessing and Visualization

An image stack can be visualized on a computer with two different software products. The first one, called Leica LAS AF Vers. 3.1.0, is an application that can visualize the stack in layers. One extracted image of a single layer is shown in Fig. 3.34. The software gives the possibility to scroll through the tissue's layers easily. The second software program (Amira Vers. 5.3.3 by Visage Imaging Inc.) was used for building 3-D reconstructions of the stack. After opening the file, see Fig. 3.35, the first appearance of the whole 3-D reconstruction is not very informative.

In order to perform an analysis of the obtained image stacks, it was necessary to cut the stack into smaller slices (at least one third of the initial length). Thereafter, some more image preprocessing, e.g. noise or Gaussian filter, were performed to achieve a better visualization. Figure 3.36 shows an example of such a smaller piece of adipose tissue, after the image preprocessing stages were performed. A particularity of this certain specimen in Fig. 3.36 is the collagen band (a special variation of an interlobular septa) that spreads through the whole thickness of the specimen.

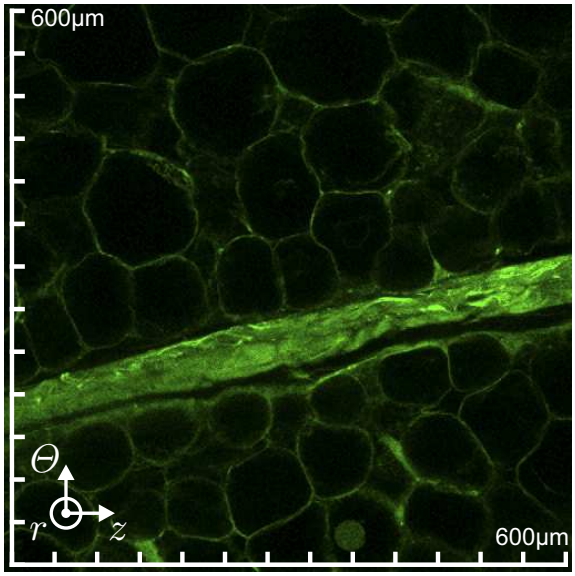

Figure 3.34.: Image showing a single layer of the MPM measurement of specimen no. VII visualized in Amira. The viewed area is $620 \times 620 \mu\mathrm{m}$

Figure 3.35.: Image stack into the 3-D reconstruction software is shown. One can see very good that the intensity is decreasing toward the r-direction.

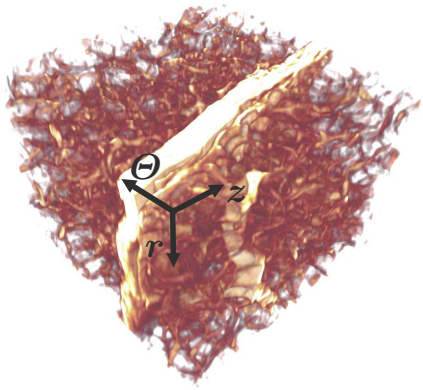

Figure 3.36.: Image stack after performing the graphical preprocessing work shown in the 3-D reconstruction software. A distinct difference in between the two image stacks is notable.

3.3.2. Angle of Interlobular Septa

Table 3.6.: Mean value and standard deviation (SD) of the three angles of the interlobular septa within the human.

	MEAN $^\circ$	SD $^\circ$
ϕ	24.1	15.1
ψ	14.6	7.6
ϑ	49.3	13.5

After finishing the preparation of the images it was possible to see the interlobular septa very well (see Fig. 3.36). The results of the measured as well as the calculated angle, is shown in Tab. 3.6. Figure 3.37 shows a graphical illustration of the results. These results show that the special fibers are situated within the body towards the head, like we expected, with a small angle and are rotate to one side (left or right side) with an even smaller angle.

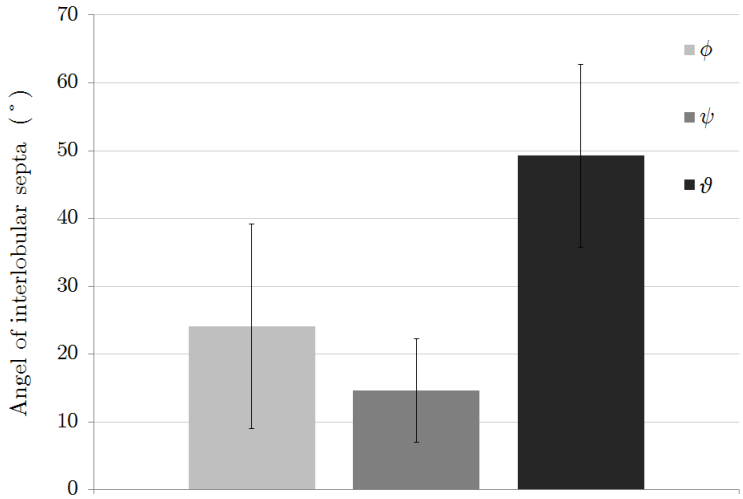

Figure 3.37.: Results to the analyses of the measuring of the angle of the interlobular septa within the human adipose tissue.

4. Discussion

Human abdominal adipose tissue is already used in clinical practice as a material for reconstructions in plastic surgery, hardly no multi-axial research of the mechanical behavior has ever been conducted. Plastic surgery will become more and more important for society, therefore it is absolutely inevitable to gain more relevant data of this type of tissue. Therefore, this study shows biomechanical data obtained for human adipose tissue from biaxial tensile and triaxial shear testing. The human adipose tissue has been investigated in a couple of research studies.

Because of these facts it is difficult to compare results of past investigation groups with those of this project. The acquired data intended to be fitted to a non-linear constitutive model. Afterward, the material model with the gained parameters might be used in FEM simulations. This can further lead to a software that may help doctors visualize the issues and the chosen medical intervention and support their decisions. In this work 17 different samples from two institutions were investigated. It was possible to conduct triaxial shear tests for almost all samples (in sum 16). Due to the larger specimen size we could only obtain the biaxial tension behavior for 14 samples.

Due to fact that the tissue was assumed to be linear-elastic and isotropic, it was decided to take into account the anisotropy of the tissue as well as the non-linearity. The result of the biaxial tension tests showed that the longitudinal direction is stiffer for smaller stretch values. If the stretch increases and exceeds 15% the transversal direction becomes stiffer than the longitudinal. Further, we detected that the stress magnitudes during dynamic tests, are smaller for all three directions than for quasi-static tests. The results of Comley and Fleck (2009) showed that adipose tissue becomes stiffer for a test at higher strain rates. The reason of our contrary results could be explained by the too low capturing frames-per-seconds achieved with our digital camera. A new camera is now installed to increase the quality of the results.

A further limitation noticed was the slippage of the tissue out of the clamps. The fixation of a specimen is a important point for testing all sorts of soft biological tissues. In our case, the mounting of the adipose tissue was tricky because of the tissue's very loose structure, e.g. it was not possible to use hooks like for arteries. Maybe there are other more satisfying solutions than using super glue. Another problem was that the specimen sometimes expanded immediately after contact with the warm PBS solution. In this case to adjust the focus of the video-extensometer was very difficult. If it was possible to fix the limitations with the focus of the video-extensometer, another future tests could be performed.

From the triaxial shear test data were acquired including four values for the shear test (positive, negative direction, and mean values as well as the energy dissipation); two for

the relaxation and one for the compression test. The results of the shear test in the positive and negative direction show that the absolute magnitudes do not correspond to each other. It appears that shearing the specimen in negative directions causes higher stresses than in positive directions. The $r\theta$- and rz-shear modes remain the modes with the lowest stress value at all shear strains, both for positive and negative direction (hence also for the mean value). The magnitudes lie about 40 to 50% lower than for the maximum shear stresses. The relaxation time are within the same range for all shear modes. The same characteristic can be observed for the PtoP-value. The dissipated energy appear to be the same level for each shear mode at the four different amounts of strain. At 40% and especially for 50% amount of shear the dissipated energy, on the one hand is the largest with 8 μNm in θz-direction, on the other the smallest with 5.8 μNm in θr-direction. The energy dissipation from 20% shear to 50% shear has increased to approximately the fourfold of its initial magnitudes. The compression test distinctively showed that the θ-direction is the stiffest and z-direction is the softest under compression. Thereby, the stress magnitude of the stiffest compared to the softest is double. Further, the r-direction is 50% decreased in comparison to the maximum in θ-direction. In summary, the results of the triaxial shear tests show that human abdominal adipose tissue is non-linear and anisotropic.

A problem occurred at the relaxation test for some of the specimens. It appeared that the relaxation time is higher than the actual testing time of 350 s. These results might be caused by an error during the test, which has not yet been figured out. Therefore, the results that included such large relaxation times were neglected.

Usually people would assume a correlation between the BMI or age of the donors. Hence we tried to figure out whether there did exist a correlation between the maximum stress values in one of the directions at biaxial tension or triaxial shear test. The stress magnitudes did not correlate with the BMI nor with the age of the donators for all stretches at the biaxial tensile test. The same effect was observed for all shear modes at 20 and 30% shear strain. A statistically significant positive correlation in the positive shear direction was observed for $z\theta$-mode at 40% shear amount between the age and absolute stress values (r$= 0.42$,p$= 0.04$) and for the θr-mode between the BMI and the absolute stress values (r$=$ 0.049,p$= 0.02$), respectively. For 50% shear strain this correlation was also notice at the same shear modes as for 40% (age at $z\theta$: r$= 0.048$,p$= 0.02$; BMI at θr: r$= 0.064$,p$= 0.01$). Hence there appears to be a correlation between the age and the stress in $z\theta$- and between the BMI and the stress in θr-mode, respectively, at higher shear strains. This positive correlation between the age and the shear stress in $z\theta$-mode could mean that the amount of collagen fibers in the direction of the interlobular septa increases. The correlation between BMI and shear stress in θr-direction might go along with an extended intergrowth of the collagen fibers for more obese people.

The MPM investigations showed good results to get an overview of the microstructure of human abdominal adipose tissue. The interlobular septa are orientated as previously assumed. The angle ϕ is 60% larger than ψ and has half the size of ϑ, i.e. the orientation in the human body lies in the longitudinal direction with a slight angle to the back and to the side of the body axis. The results could be improved by increasing the observed

volume as well as the number of specimens. Specimens that were already tested in triaxial shear or biaxial tension should be preferred investigated, to link the results of two investigations. Additionally, it might be possible to investigate and visualize damages, caused by the mechanical test. The results of the MPM investigation correspond approximately to the obtained data of the biaxial tension and triaxial shear tests.

5. Conclusion

The investigated tissue exhibits clearly as a mechanically non-linear as well as anisotropic tissue. The study shows a positive significant correlation between the shear stress in $z\theta$-direction and the age. Moreover, there is a positive correlation observed between the shear stress value in θr-direction and the BMI. This mechanical and structural is intended to be used for material parameter identification and following soft tissue computer simulations. This simulations can be used to investigate the stress condition during normal life and some more simulations. Another outcome will the usage in clinical practice for planning optimal plastic reconstruction surgery procedures as well as helping the patient understand the planned surgical interventions.

Bibliography

D R Abrahamson. Recent studies on the structure and pathology of basement membranes. *Journal of Pathology*, 149(4):257–278, 1986.

K Chen and J D Weiland. Mechanical Properties of Orbital Fat and Its Encapsulating Connective Tissue. *Journal of Biomechanical Engineering*, 133:64505, 2011.

K Comley and N A Fleck. The mechanical response of porcine adipose tissue. (June): 1–30, 2009.

K Comley and N A Fleck. A micromechanical model for the Young's modulus of adipose tissue. *International Journal of Solids and Structures*, 47:2982–2990, 2010.

M Geerligs, G W M Peters, P A J Ackermans, C W J Oomens, and F P T Baaijens. Linear viscoelastic behavior of subcutaneous adipose tissue. *Biorheology*, 45:677–688, 2008.

G A Holzapfel, T C Gasser, and R W Ogden. A new constitutive framework for arterial wall mechanics and a comparative study of material models. 61:1–48, 2000.

J D Humphrey, R K Strumpf, and F C P YIN. Biaxial mechanical behavior of excised ventricular epicardium Humphrey Strumpf Yin 1990 AJP.pdf. page 8, 1990.

J E Miller-Young, N A Duncan, and G Baroud. Material properties of the human calcaneal fat pad in compression: experiment and theory. *Journal of biomechanics*, 35(12):1523–1531, December 2002. ISSN 0021-9290. URL `http://www.ncbi.nlm.nih.gov/pubmed/12445605`.

I Nakajima, T Yamaguchi, K Ozutsumi, and H Aso. Adipose tissue extracellular matrix: newly organized by adipocytes during differentiation. *Differentiation; research in biological diversity*, 63(4):193–200, August 1998. ISSN 0301-4681. doi: 10.1111/j.1432-0436.1998.00193.x. URL `http://www.ncbi.nlm.nih.gov/pubmed/9745710`.

A Samani, J Zubovits, and D Plewes. Elastic moduli of normal and pathological human breast tissues: an inversion-technique-based investigation of 169 samples. *Physics in Medicine and Biology*, 52:1565–1576, 2007.

Training Modules SEER. Skin cancer: Melanoma. In *U. S. National Institutes of Health, National Cancer Institute.*, 2013. URL `http://training.seer.cancer.gov/`.

C S Tam, V Lecoultre, and E Ravussin. Brown adipose tissue: mechanisms and potential therapeutic targets. *Circulation*, 125(22):2782–91, June 2012. ISSN 1524-4539. doi: 10.1161/CIRCULATIONAHA.111.042929. URL http://circ.ahajournals.org/cgi/content/long/125/22/2782.

J Z Wu, R G Cutlip, M E Andrew, and R G Dong. Simultaneous determination of the nonlinear-elastic properties of skin and subcutaneous tissue in unconfined compression tests. *Skin Research and Technology*, 13:34–42, 2007.

A. Appendix

In the following box-whiskers plots of all calculated data are shown.

A.1. Biaxial Tension

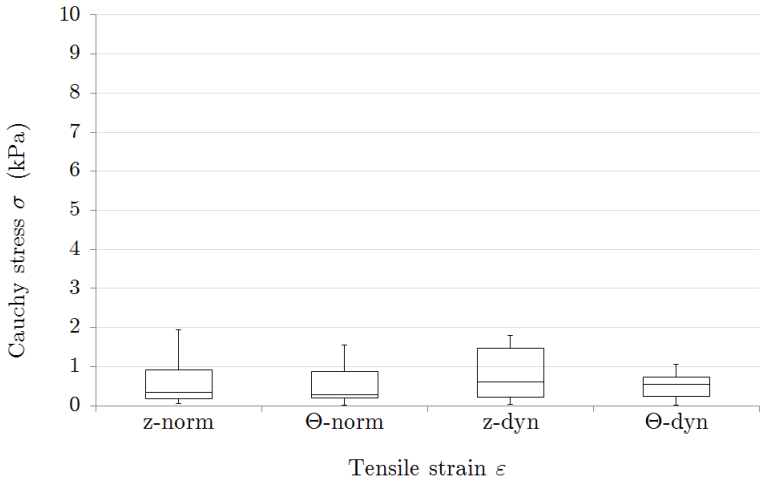

Figure A.1.: Diagram of the not normal distributed data of the biaxial tension test. Showing the data for dynamic and quasi-static test at 5% stretch.

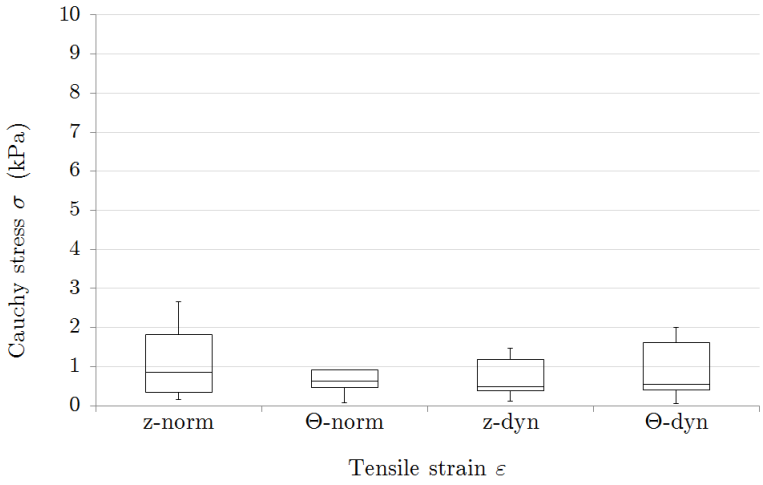

Figure A.2.: Diagram of the not normal distributed data of the biaxial tension test. Showing the data for dynamic and quasi-static test at 10% stretch.

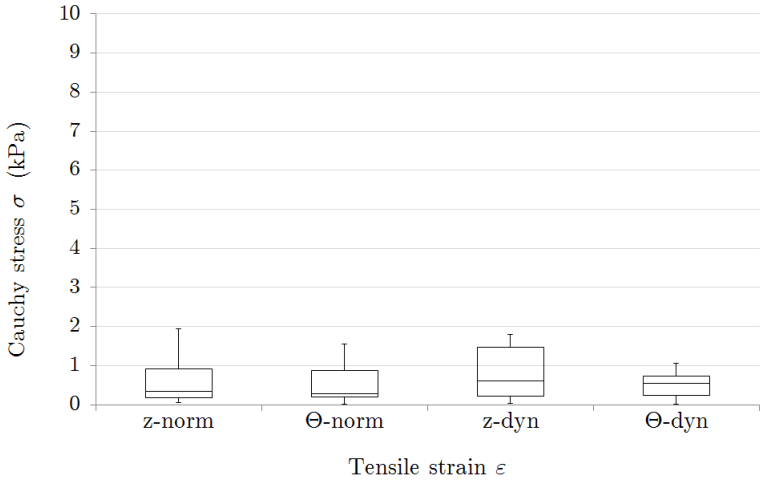

Figure A.3.: Diagram of the not normal distributed data of the biaxial tension test. Showing the data for dynamic and quasi-static test at 15% stretch.

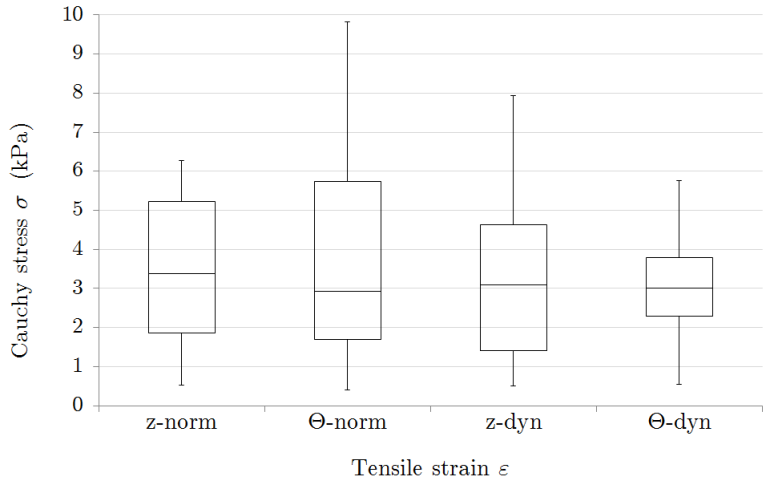

Figure A.4.: Diagram of the not normal distributed data of the biaxial tension test. Showing the data for dynamic and quasi-static test at 20% stretch.

A.2. Triaxial Shear

A.2.1. Positive Direction

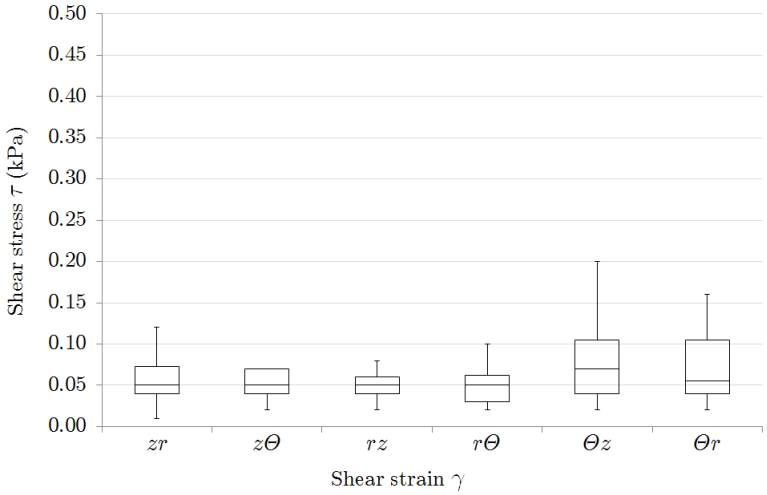

Figure A.5.: Data for 20% shear in positive direction. Results are not normal distributed and therefore shown in box plot.

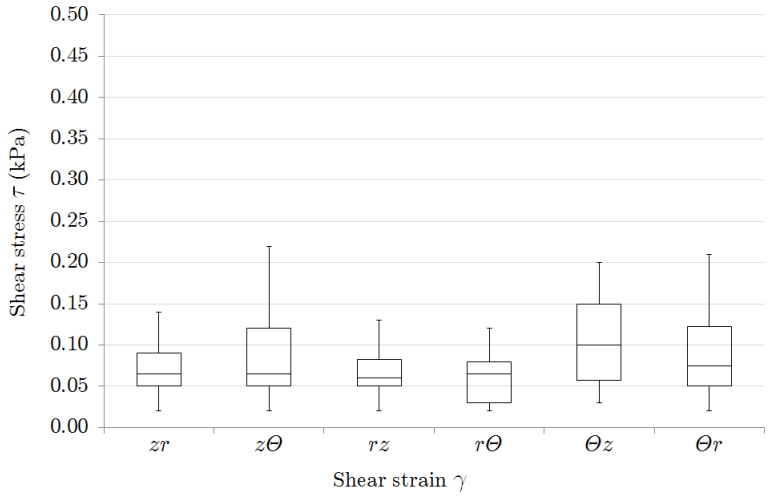

Figure A.6.: Data for 30% shear in positive direction. Results are not normal distributed and therefore shown in box plot.

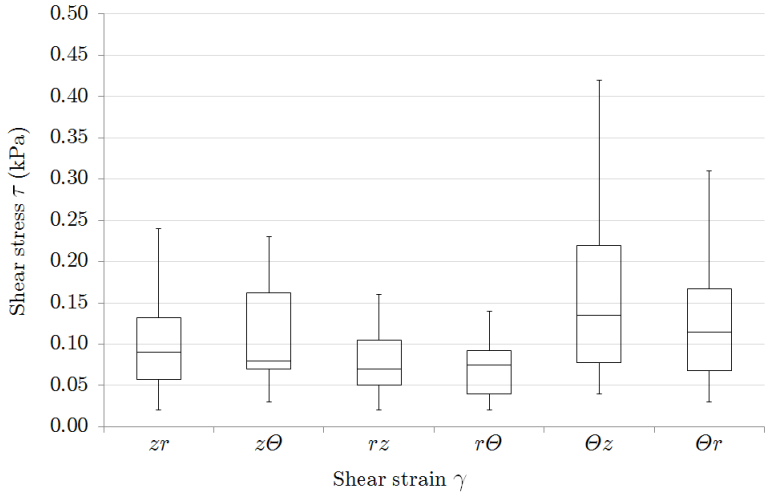

Figure A.7.: Data for 40% shear in positive direction. Results are not normal distributed and therefore shown in box plot.

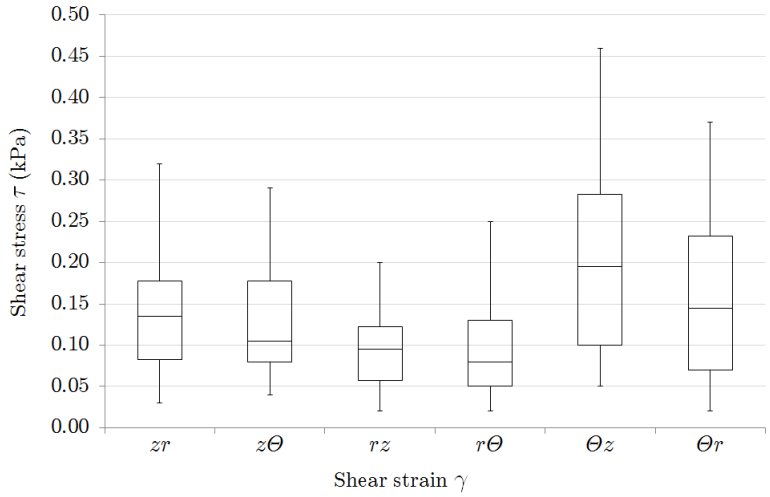

Figure A.8.: Data for 50% shear in positive direction. Results are not normal distributed and therefore shown in box plot.

A.2.2. Negative Direction

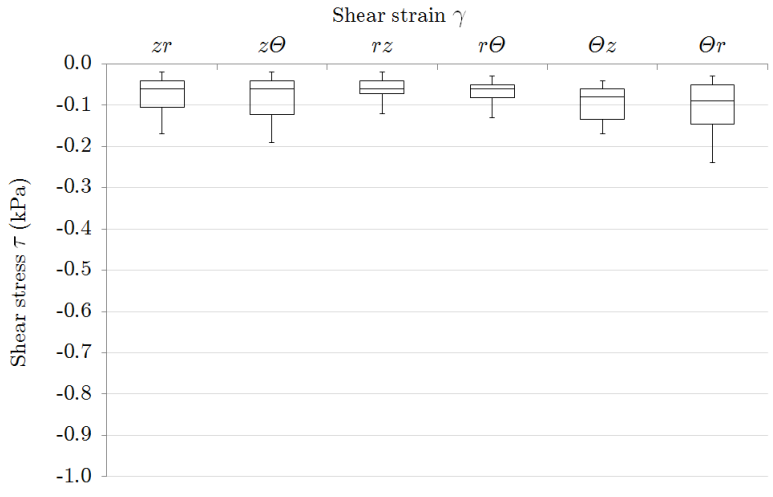

Figure A.9.: Not normal distributed data of the 20% shear in negative direction.

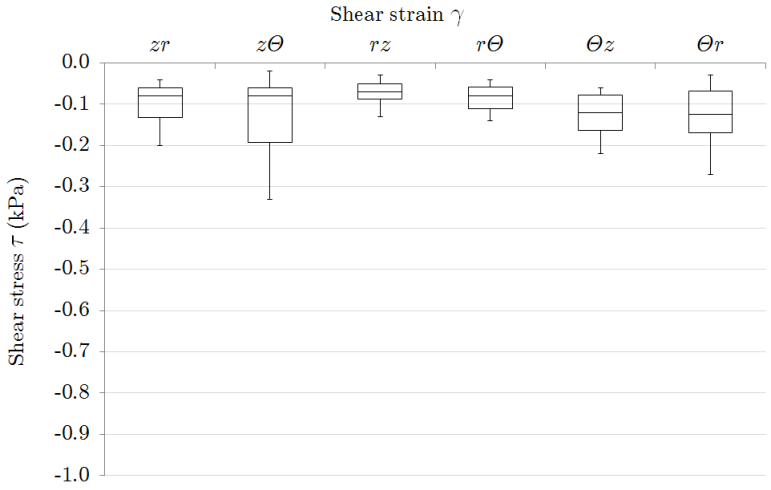

Figure A.10.: Not normal distributed data of the 30% shear in negative direction.

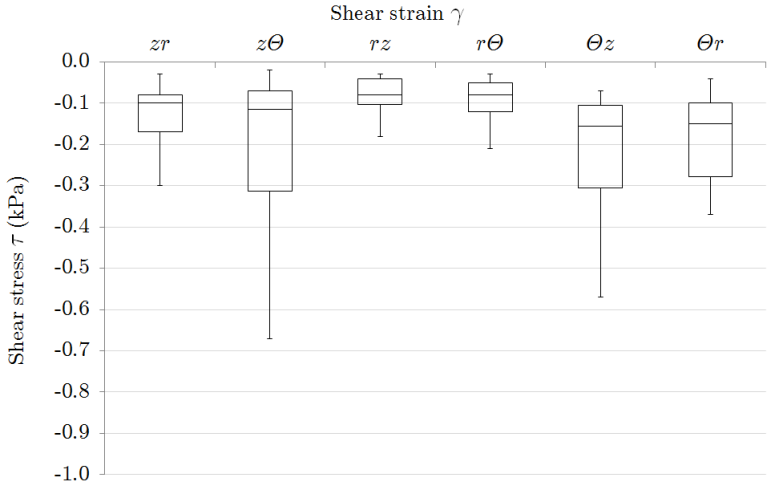

Figure A.11.: Not normal distributed data of the 40% shear in negative direction.

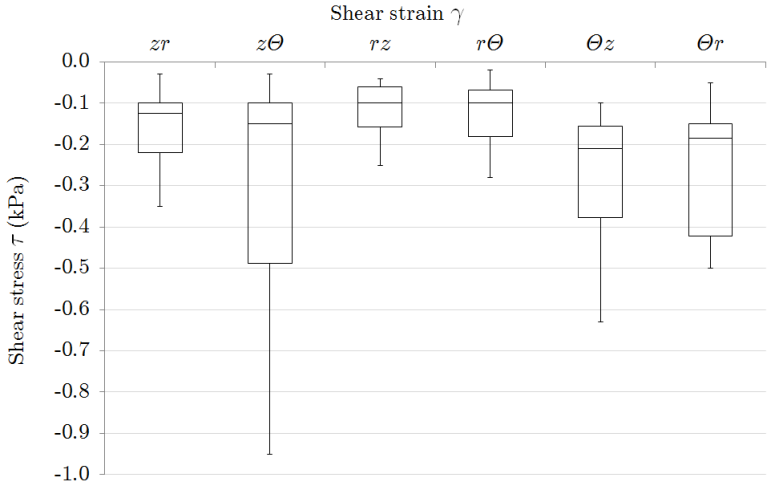

Figure A.12.: Not normal distributed data of the 50% shear in negative direction.

A.2.3. Mean of Both Directions

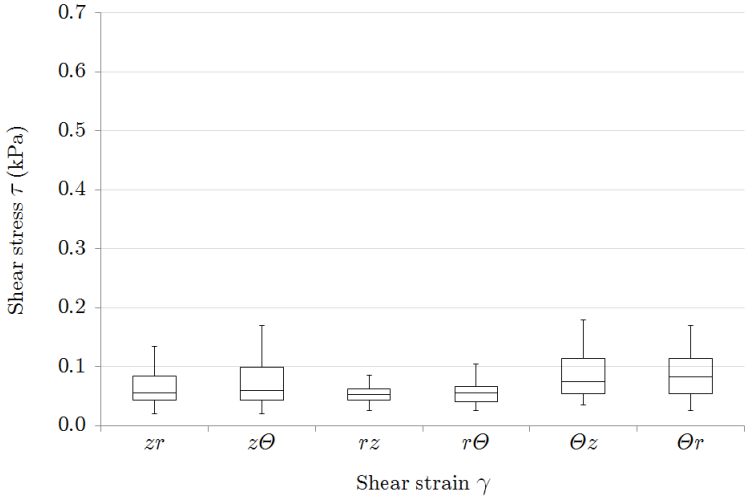

Figure A.13.: Mean values for 20% shear in both-direction.

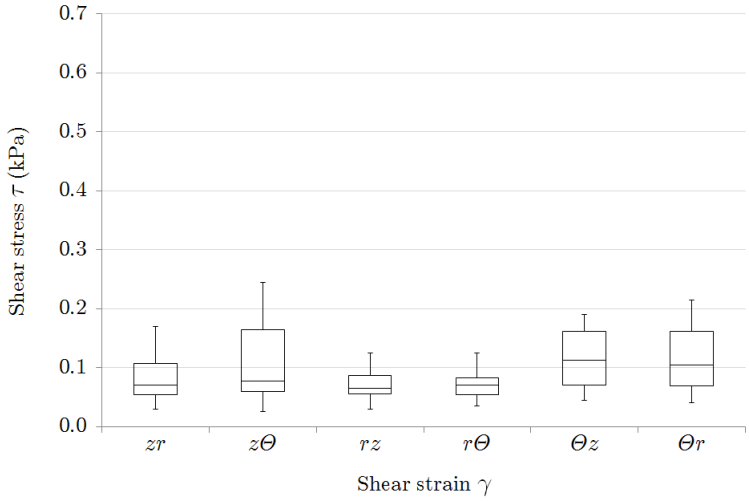

Figure A.14.: Mean values for 30% shear in both-direction.

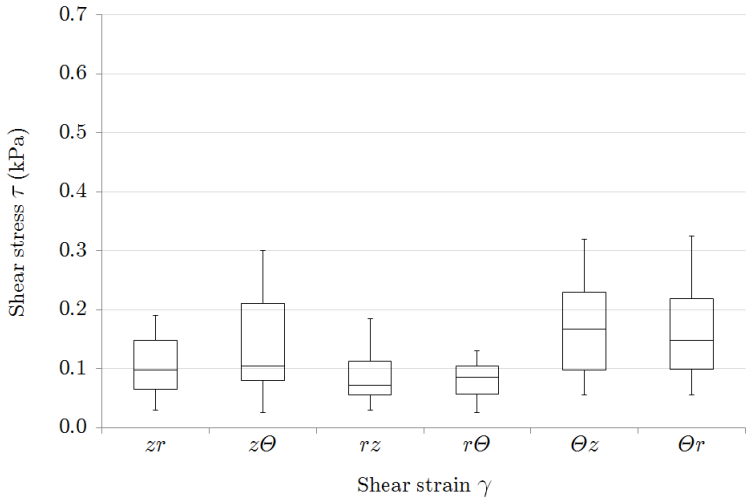

Figure A.15.: Mean values for 40% shear in both-direction.

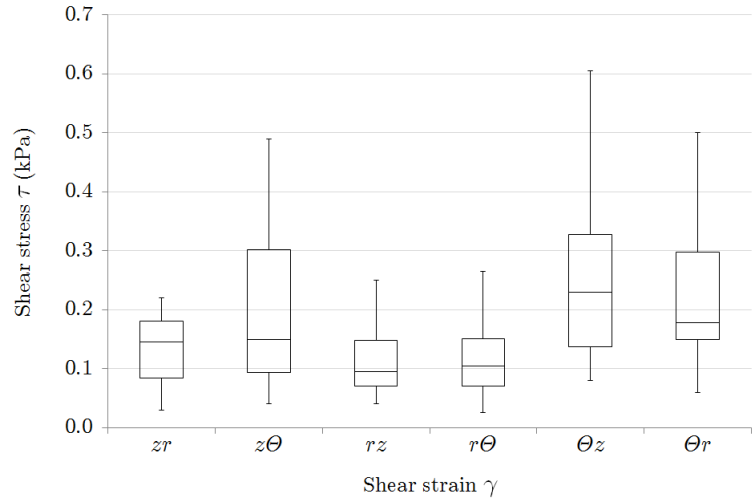

Figure A.16.: Mean values for 50% shear in both-direction.

A.2.4. Relaxation Test

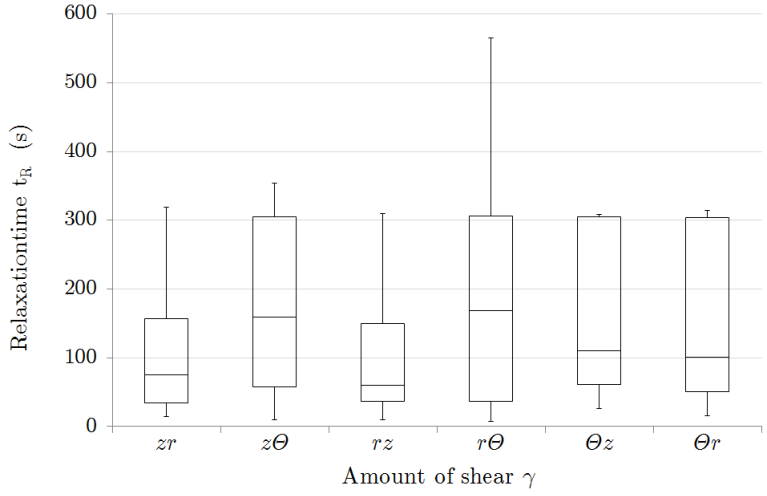

Figure A.17.: Diagram of the not normal distributed data of the relaxation time.

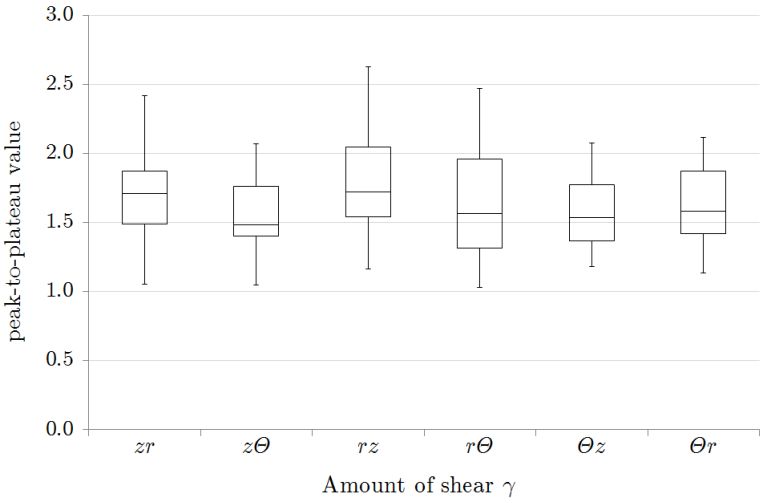

Figure A.18.: Diagram of the not normal distributed data of the peak-to-plateau-value.

A.2.5. Compression Test

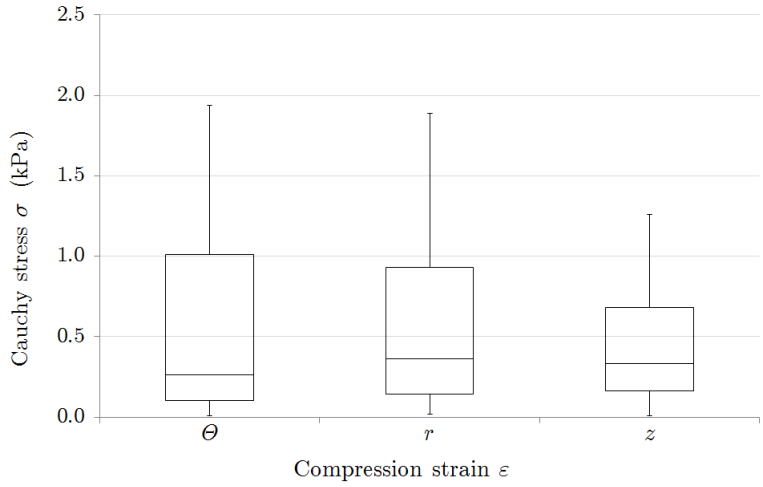

Figure A.19.: Diagram of the not normal distributed data of the compression stresses.

A.2.6. Dissipated Energy

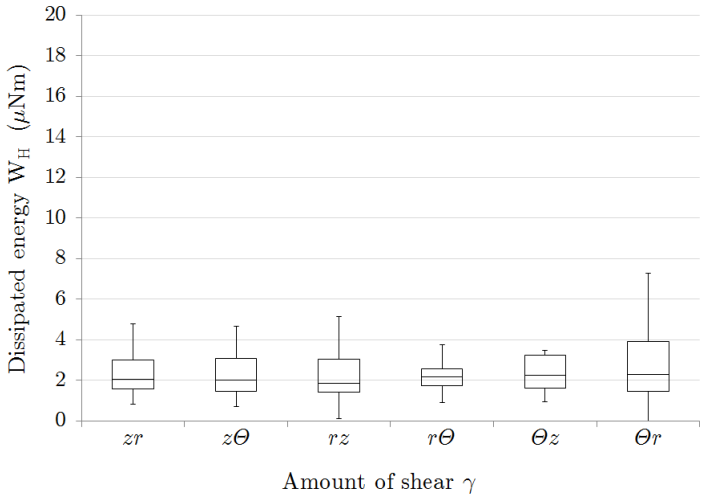

Figure A.20.: Dissipated energy in form of a box plot for 20% shear.

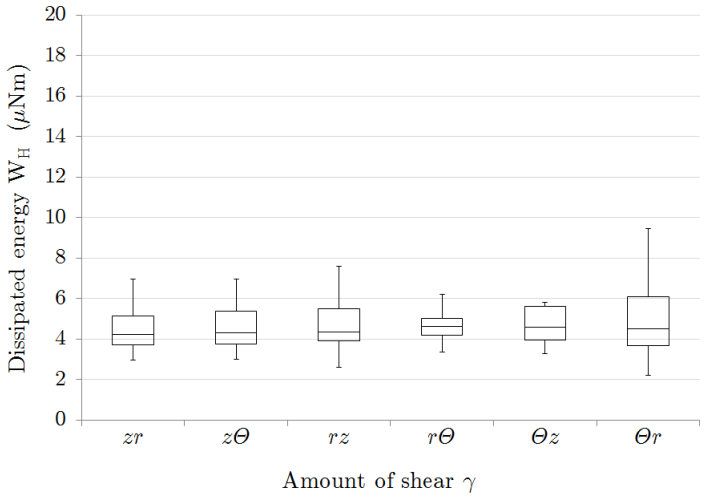

Figure A.21.: Dissipated energy in form of a box plot for 30% shear.

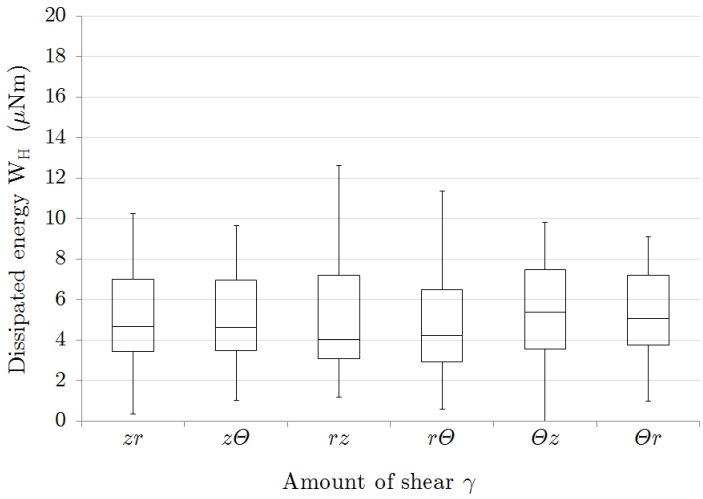

Figure A.22.: Dissipated energy in form of a box plot for 40% shear.

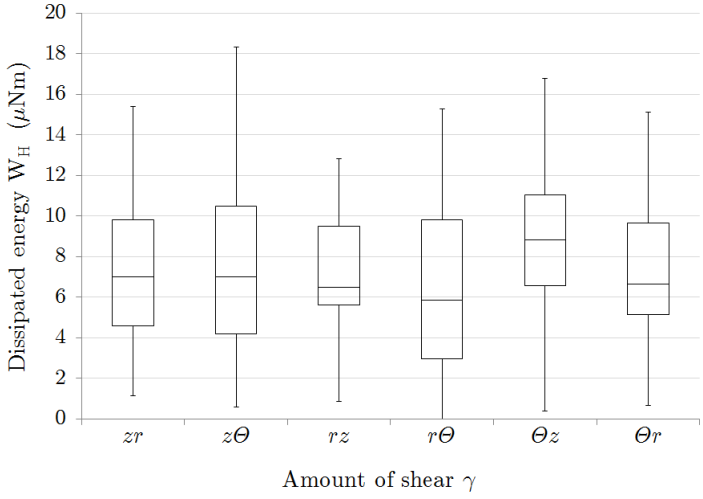

Figure A.23.: Dissipated energy in form of a box plot for 50% shear.

A.3. Angular of Interlobular Septa

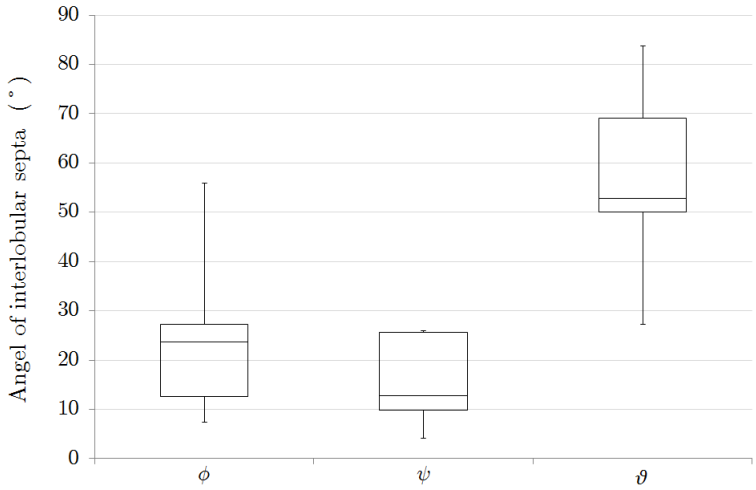

Figure A.24.: Diagram of the not normal distributed data of the angle of the interlobular septa.

Statutory Declaration

I declare that I have authored this Thesis independently, that I have not used other than the declared sources/resources, and that I have explicitly marked all material, which has been quoted by the relevant reference.

date	signature